Joint Transceiving and Reflecting Design for Intelligent Reflecting Surface Aided Wireless Power Transfer

Qingdong Yue, Jie Hu, *Senior Member, IEEE*, Kun Yang, *Fellow, IEEE*, Qin Yu *Member, IEEE*

***Abstract*—In an intelligent reflecting surface (IRS) aided wireless power transfer (WPT) system, a practical architecture of an energy receiver (ER) is proposed, which includes multiple receive antennas, an analog energy combiner, a power splitter and multiple energy harvesters. In order to maximise the output direct-current (DC) power, the transmit beamformer of the transmitter, the passive beamformer of the IRS, the energy combiner, and the power splitter of the ER are jointly optimised. The optimisation problem is equivalently divided into two sub-problems, which independently maximises the input RF power and the output DC power of the energy harvesters, respectively. A successive linear approximation (SLA) based algorithm with a low complexity is proposed to maximise the input RF power to the energy harvesters, which converges to a Karush-Kuhn-Tucker (KKT) point. We also propose an improved greedy randomized adaptive search procedure (I-GRASP) based algorithm having better performance to maximise the input RF power. Furthermore, the optimal power splitter for maximising the output DC power of the energy harvesters is derived in closed-form. The numerical results are provided to verify the performance advantage of the IRS-aided WPT and to demonstrate that conceiving the optimised energy combiner achieves better WPT performance than the deterministic counterpart.**

***Index Terms*—Wireless power transfer (WPT), Intelligent reflecting surface (IRS), Power splitter, MIMO, Energy harvester architecture, Multiple non-linear rectifers.**

I. Introduction

Low-power Internet-of-Everythings (IoE) devices for sensing, small-scale computation and communication can be wireless powered by ratio frequency (RF) signals in wearable medical applications and environments monitoring. The number of IoE devices (e.g., electronic tablets, sensors, wearables, and so on) is anticipated to grow from 7 billion in 2018 to 22 billion by 2025. A tremendous number of wireless devices thus require a scalable solution for perpetual energy supply, which can be realised by RF based wireless power transfer (WPT) in the future energy self-sustainable 6G [1]. With the rapid growth of the low-power IoE devices, energy supply of these are usually powered by embedded batteries. However, quickly drained batteries largely limit performance of IoE devices. Therefore, RF signals are reliable to transfer wireless power to these devices. However, due to the severe channel attenuation during the wireless signal propagation, the transmitter has to suffer from very high energy consumption in order to maintain satisfactory WPT in a reasonable coverage [2], [3]. For the sake of counteracting the channel attenuation, multiple-input-multiple-output (MIMO) system has been exploited for providing substantial spatial gains in WPT .

Specifically, Zhong *et al.* [4] studied WPT in the beamspace of a large-scale MIMO system by conceiving a linear energy harvester. However, Boshkovska *et al.* [5] proposed a practical model for characterising the saturation and non-linearity of diode based energy harvesters. Xiong *et al.* [6] explored the rate-energy region of SWIPT in a MIMO aided broadcasting system with these non-linear energy harvesters. By considering the saturation phenomenon of a practical non-linear energy harvester, Lu *et al.* [7] proposed a novel power splitting based energy receiver in a MISO-SWIPT system. The received RF power were split into several portions to avoid the saturation region of non-linear energy harvesters. As for a MIMO-SWIPT system, how to effectively utilise the spatial gain in improving the WPT with a practical energy harvester is still an open problem.

Most of existing works focus on either the transmit beamformer or the precoder design for dedicated WPT and the SWIPT [8]. However, signal processing for the performance improvement of the energy harvesters has been largely ignored. The key question is how do we deal with the multiple energy flows gleaned by multiple antennas of energy harvester? No matter what kinds of energy harvesters we conceive, linear or non-linear one, the rectified output DC power is mainly determined by the input RF power. Most of MIMO-SWIPT or MIMO-WPT related works [9], [10] presumed that the total RF power is the sum of the RF power gleaned by every antenna. However, this is impractical in terms of hardware implementation. In order to reduce the hardware complexity, Linnartz *et al.* [11] proposed a more practical a energy harvester with multiple antennas. By adjusting the phases of the RF signals received by the multiple antennas in the analog domain, they were constructively combined and rectified by a single energy harvester. Shanpu *et al.* [12] considered the RF combining by adopting the

Qingdong Yue, Jie Hu and Qin Yu are all with the Yangtze Delta Region Institute (Huzhou) and the School of Information and Communication Engineering, University of Electronic Science and Technology of China, Huzhou, 313001, China, email: qdyue1588@163.com, hujie@uestc.edu.cn and yuqin@uestc.edu.cn.

Kun Yang is with the School of Information and Communication Engineering, University of Electronic Science and Technology of China, email: kunyang@uestc.edu.cn.

The authors would like to thank the financial support of National Natural Science Foundation of China (No. 61971102), that of Sichuan Science and Technology Program (No. 2022YFH0022), that of MOST Major Research and Development Project (Grant No.: 2021YFB2900204), that of Sichuan Major R&D Project (Grant No.: 22QYCX0168), that of the Municipal Government of Quzhou (Grant No.: 2022D031), and that of Key Research and Development Program of Zhejiang Province (No. 2022C01093).

nonlinear energy harvester. However, this energy harvester is modelled by Taylor-expansion, which is suitable for only a small region. Therefore, the optimal design of the energy combiner by considering a more accurate energy harvesting model still worth further discussion.

Intelligent reflecting surface (IRS) assisted wireless communication emerges as a key enabling technique for next generation of wireless communications [13]. Pan *et al.* [14] introduced IRS from different aspects, such as applications, challenges and future research directions. An IRS is composed of a large number of low-cost reflecting elements, each of which is capable of passively reflecting RF signals by adjusting their phases in the analog domain [15]. Therefore, the resultant passive beam aims at receivers, which may substantially improve wireless communication performance by exploiting additional spatial gains. Compared to a traditional MIMO based relaying system, the IRS-aided MIMO system only passively reflect RF signals, which are emitted by a transmitter. It does not invoke any active power-consuming RF chains, which substantially reduces its hardware complexity and energy-consumption. Furthermore, due to the sophisticate signal processing at relays, a conventional relaying system mostly spent an additional transmission frames for forwarding information to the destination, which may thus reduce the end-to-end throughput. However, the RF signals can be instantaneously reflected by the IRS, which do not need another transmission frame. Moreover, due to the severe path-loss of wireless channels, line-of-sight (LoS) is preferred by both the WPT and the SWIPT.

Specifically, Bai *et al.* [16] studied optimal resource allocation in an IRS aided mobile edge computing system. Pan *et al.* [17] studied an IRS-aided MIMO-SWIPT system. They maximised the weighted sum-rate of multiple information receivers by ing the transmit precoder at the transmitter and the passive reflecting beamformer at the IRS, while satisfying the energy harvesting requirements of all the energy receivers. Lyu *et al.* [18] investigated an IRS assisted wireless powered communication network to improve both the downlink WPT and the uplink wireless information transfer (WIT) performance. An up-link sum-rate maximisation problem was formulated by jointly optimising the time scheduling and the passive reflecting beamformer of the IRS. Wu *et al.* [19] studied an IRS aoptimisided MISO-SWIPT system. They aimed to maximise the weighted sum-power harvested by all the energy users (EUs) by jointly optimising the transmit percoder and the passive reflecting beamformer of the IRS, while satisfying the the individual signal-to-interference-plus-noise-ratio constraints of all the information users.

Some effective algorithms were proposed for designing the discrete phase-shifters of the IRS aided system [20]–[23]. Specifically, Wu *et al.* [20] converted the discrete phase optimisation on passive reflecting beamformer of the IRS to a linear integer programming (LIP). Gong *et al.* [21] reformulated the discrete phase optimisation to an approximate "quadratic assignment programming" (QAP) problem. However, it did not satisfy the real positive quadratic coefficient requirement of the original QAP. Then, they converted the QAP to the LIP, which could be solved by a classic branch-and-bound method. However, the complexity of the branch-and-bound method exponentially grew as the number of the reflector in the IRS increased, which had almost the same complexity with the exhaustive search. Therefore, the standard branch-and-bound based algorithm was only suitable when the number of reflectors in the IRS was fewer than 30 [21]. Therefore, some sub-optimal solutions were investigated in [22], [23]. They developed an iterative algorithm for alternatively optimising every reflector, when the other peers are fixed.

In a nut shell, the existing works on the design of IRS-aided WPT system has the following drawbacks:

- They only focused on the joint design of the active transmit beamformer and the passive reflecting beamformer, where the energy receivers (ERs) were only equipped with a single antenna. Multiple antennas aided ERs were not considered.
- A practical architecture of ERs was never investigated. The potential performance gains incurred by multiple antennas, multiple energy harvesters and multiple phase-shifters were totally ignored. The non-linear characteristics of practical energy harvesters were never exploited for the ER design.
- The phase-shifters of the IRS and the transmit beamformer of the transmitter in some works [19], [24] were jointly designed by exploiting semi-definite relaxation (SDR) with a very high computational complexity, which was unaffordable in a practical WPT system. Moreover, the convergence of the SDR based algorithm cannot be ensured. Some work [25] proposed block coordinate descent (BCD) and complex circle manifold (CCM) algorithms, both of which has high complexity. Some works [20], [21] designed the phase-shifters of the IRS by converting to LIP and exploiting branch-and-bound based algorithm, whose complexity exponentially grew as the number of the reflector in the IRS increased. Furthermore, Some works [22], [23] proposed an iterative algorithm, whose performance is relied on the randomly initialised solution. The complexity of the iterative algorithm is also pretty high.

In order to overcome the above-mentioned drawbacks, our novel contributions are summarize as below:

- We investigate an IRS-aided WPT system. A practical architecture of an ER is proposed, which consists of an energy combiner, a power splitter and a number of energy harvesters. Specifically, multiple receive antennas and a number of low-resolution analog phase-shifters constitute the energy combiner, which aims for optimally combining the RF signals received by multiple antennas. In order to avoid the saturation of non-linear energy harvesters, the received RF power is split in the power domain before inputting to multiple energy harvesters.
- We jointly design the active transmit beamformer of the transmitter, the passive reflecting beamformer of the IRS, the energy combiner and the power splitter of the ER for the sake of maximising the output DC power. The resolution constraints on the phase-shifters of the IRS and those of the ER are considered. The original optimisation

problem is equivalently divided into two sub-problems, which maximises the input RF power and the output DC power, respectively.

- A successive linear approximation (SLA) based algorithm is proposed to maximise the input RF power. After exploiting the minorize maximisation (MM) method, we convert the optimisation to its convex counterpart, while both optimisations have the same optimal solution. By exploiting the Lagrangian duality, the passive reflect beamformer of the IRS is derived in closed-form, when the other variables are given. Similarly, the active transmit beamformer and the energy combiner are also derived in closed-form, when the passive reflect beamformer is given. All the closed-form solutions result in a very low complexity which can be readily implemented in practice. The discrete solution is obtained from the continuous one, which converges to a Karush-Kuhn-Tucker (KKT) point and guarantees a local optimum.
- The input RF power maximisation problem is also solved by another 0-1 quadratic assignment programming (QAP). We firstly reformulated it as a standard QAP with real and positive quadratic coefficients. An improved greedy randomize adaptive search procedure (I-GRASP) based algorithm is proposed to jointly optimise the active transmit beamformer, passive reflecting beamformer and energy combiner. This algorithm achieves a better WPT performance but pays the price of a higher complexity.
- The optimal power splitting ratio of the ER is also obtained in closed-form. Therefore, the computational complexity of our joint design is significantly reduced.
- Numerical results verify the performance advantage of our proposed algorithms. The I-GRASP algorithm has the best performance compared to other counterparts. The SLA algorithm has the lowest complexity, while its performance is close to that of I-GRASP algorithm. The design principle of an ER is summarized as follow: The deterministic energy combiner (DEC) has the lowest hardware-complexity but it also has the lowest energy harvesting performance; The optimised energy combiner (OEC) with a uniform power splitter has the best energy harvesting performance, when the received RF power is high, but it renders a higher hardware-complexity. The OEC-only based ER may achieves satisfactory energy harvesting performance, when the received RF power is low.

The rest paper is organised as follows: System model and problem formulation are introduced in Section II. Two algorithms are proposed to maximise the input RF power in Section III and Section IV, respectively, while the optimal power splitter ratio is derived in Section V. After presenting pivotal numerical results in Section VI, our paper is finally concluded in Section VII.

Notation: $(\cdot)^H$ denotes transpose-conjugate operations. $|a|$ and $||\mathbf{a}||_2$ are the magnitude and norm of a scalar a and vector $\mathbf{a}$. $\mathbf{A}(i,j)$ represents the element at i-th row and j-th column in $\mathbf{A}$. vec$(\mathbf{a})$ is the vectorization of vector $\mathbf{a}$. $diag(\mathbf{A})$ is the vector diagonalized by the diagonal matrix $\mathbf{A}$. $\max(\mathbf{A})$ is the maximum value of the matrix $\mathbf{A}$.

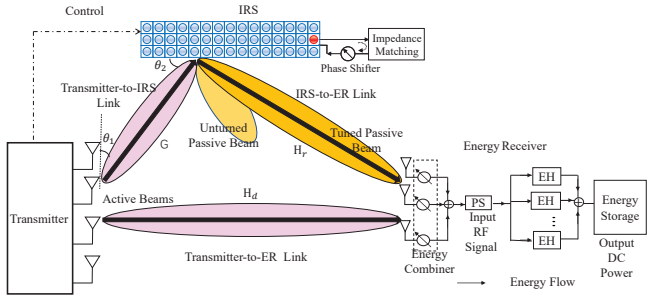

Fig. 1. IRS added MIMO system.

II. System Model and Problem Formulation

A. IRS-Aided WPT System

The IRS aided WPT system has a single transmitter equipped with $N_t > 1$ antennas, a single energy receiver (ER) equipped with $N_r > 1$ antennas and an IRS equipped with $M > 1$ passive reflectors. The wireless channel from the transmitter to the IRS, that from the IRS to the ER and that from the transmitter to the ER are denoted as $\mathbf{G} \in \mathbb{C}^{N_t \times M}$, $\mathbf{H}_r \in \mathbb{C}^{M \times N_r}$ and $\mathbf{H}_d \in \mathbb{C}^{N_t \times N_r}$, respectively, as illustrated in Fig.1.

The transmit signal for the dedicated WPT is expressed as $\mathbf{x} = \mathbf{f}s$ where s is an 1×1 deterministic signal satisfying $||s|| = 1$ and $\mathbf{f} \in \mathbb{C}^{N_t \times 1}$ is the active transmit beamformer. Here we adopt a the discrete complex baseband signal model. We assume that the channel response stays constant during the coherence time. Note that the energy of a passband signal is equal to its baseband version. The only difference is their carrier frequency. Therefore, this does not affect our calculation on the WPT performance. Let us denote the phase-shifter of the m-th passive reflector of the IRS by $\phi_m \in \mathcal{F}$, where $\mathcal{F} \triangleq \{e^{\frac{j2\pi b}{2^B}} | b = 1, 2, \cdots, 2^B\}$. Therefore, the passive reflector simply multiplies the incident multi-path signals by ϕ_m and it then reflects the adjusted signal to the ER. The ER receives the RF signal directly transmitted by the transmitter and that reflected by the IRS, which is then expressed as

$$\mathbf{y} = (\mathbf{H}_d + \mathbf{G}\mathbf{\Phi}\mathbf{H}_r)\mathbf{f}\mathbf{s} + \mathbf{n} \tag{1}$$

where $\mathbf{y} \in \mathbb{C}^{N_r \times 1}$ is the received RF signal, $\mathbf{\Phi} \in \mathbb{C}^{M \times M}$ is the diagonal phase-shifter matrix having $diag(\mathbf{\Phi}) = \{\beta_1\phi_1, \beta_2\phi_2, \cdots, \beta_M\phi_M\}$. Note that $\beta_m \in [0,1]$ is the amplitude reflection coefficient of the m-th passive reflector. We assume that $\beta_m = 1$ for $\forall m$, while $\mathbf{n}$ is the white noise satisfying $\mathbf{n}(i) \sim \mathcal{CN}(0, \sigma)$, for $\forall i$.

B. Practical Energy Harvester

The practical multi-antenna energy harvester contains a energy combiner, a power splitter and several energy harvesters as illustrated in Fig.1. The ER combines the multiple signals gleaned by multiple antenna into one signal stream by the analog energy combiner. The power splitter splits the RF power into several portions input into the energy harvester. Lu *et al.* [7] studied a similar energy receiver with multiple

energy harvester in order to avoid the saturation phenomenon of the RF-DC energy conversion. According to [7] the energy harvesting circuit only consists of several capacitors and resistances. It has very low hardware complexity. Therefore, multiple energy harvester can be practically integrated within a miniature device.

An energy combiner aims for constructively combining RF signals gleaned by multiple receive antennas. As shown in Fig. 1, an analog combiner is constituted by a number of analog phase-shifters to arbitrarily adjust the phase of the received RF signals. Specifically, the resultant combined signal $\hat{y}$ of the ER can be expressed as

$$\hat{y} = \mathbf{w}^H \mathbf{y} = \mathbf{w}^H (\mathbf{H}_d + \mathbf{G}\mathbf{\Phi}\mathbf{H}_r)\mathbf{f}s + \mathbf{w}^H \mathbf{n} \tag{2}$$

where $\mathbf{w} \in C^{Nr \times 1}$ satisfying $\mathbf{w}(i) \in \mathcal{W}$, where $\mathcal{W} \triangleq \{e^{\frac{j2\pi b}{2^B}} | b = 1, 2, \cdots, 2^B\}$. Given the combined signal $\hat{y}$, the resultant RF power input to the energy harvesters is expressed as

$$P_{RF} = ||\hat{y}^H \hat{y}||_2^2 = ||\mathbf{w}^H (\mathbf{H}_d + \mathbf{G}\mathbf{\Phi}\mathbf{H}_r)\mathbf{f}||_2^2. \tag{3}$$

Since all the analog-phase-shifters are optimally designed for achieving a maximum RF power, this is called optimised energy combiner (OEC).

Boshkovska *et al.* [5] found that a diode based energy harvester is non-linear model with a saturation phenomenon for rectifying the RF power to the DC one, which is expressed as

$$\Psi(P) = \frac{M}{X(1 + \exp(-a(P - b)))} - Y, \quad [Watt] \tag{4}$$

where $X = \frac{\exp(ab)}{1+\exp(ab)}$ and $Y = \frac{M}{\exp(ab)}$, P is the input RF power and $\Psi(P)$ is the output DC power. Moreover, M denotes the saturated upper-bound of the output DC power, while the constants a and b represent the joint impact of the resistances, the capacitances, and the circuit sensitivity on the rectifying process.

According to Eq. (4), the non-linear energy harvester exhibits a high energy rectifying efficiency in its non-saturation region. One of our purpose is to carefully design the power splitting strategies for the multiple energy harvesters, so that we can keep all the energy harvesters operating in the non-saturation region. Therefore, the maximum RF-DC energy conversion efficiency can be achieved.

C. Problem Formulation

Our goal is to maximise the output DC power at the ER by jointly designing the transmit beamformer $\mathbf{f}$ of the transmitter, the passive reflecting beamformer $\mathbf{\Phi}$ of IRS, the energy combiner $\mathbf{w}$ and power splitter $\boldsymbol{\rho}$ of the ER. This maximisation problem is formulated as

$$\text{(P1)}: \max_{\mathbf{w},\mathbf{f},\mathbf{\Phi},\boldsymbol{\rho}} \sum_{j=1}^{N} \Psi(\boldsymbol{\rho}(j) P_{RF}), \tag{5}$$

$$\text{s.t. } P_{RF} = ||\mathbf{w}^H (\mathbf{H}_d + \mathbf{G}\mathbf{\Phi}\mathbf{H}_r)\mathbf{f}||_2^2, \tag{5a}$$

$$||\mathbf{f}||_2^2 \leq P_t, \tag{5b}$$

$$\mathbf{w}(i) \in \mathcal{W},\ i = 1, \cdots, N_r, \tag{5c}$$

$$\mathbf{\Phi}(m, m) \in \mathcal{F},\ m = 1, \cdots, M, \tag{5d}$$

$$0 \leq \boldsymbol{\rho}(j) \leq 1,\ j = 1, \cdots, N, \tag{5e}$$

$$\sum_{j=1}^{N} \boldsymbol{\rho}(j) = 1. \tag{5f}$$

where P_{RF} in Eq. (5a) is the input RF power to the energy harvesters. An upper-bound constraint P_t is imposed on the actual transmit power of the transmitter, as expressed in (5b), while (5c) and (5d) represent the low resolution constraints on both the passive reflecting beamformer of the IRS and those of the energy combiner $\mathbf{w}$. Obviously, at the ER, the output DC power is a monotonously increasing function with respect to the input RF power P_{RF}. Therefore, P_{RF} should be as high as possible. Furthermore, the power splitter aims for ensuring the energy harvesters operating in the non-saturation region so as to maximise the output DC energy. As a result, the original optimisation problem (P1) can be equivalently decomposed into the following sub-problems (P2) and (P3).

The optimisation problem (P2) aims for maximising the received RF power P_{RF}, which is also the input RF power to the energy harvesters, by optimising the active transmit beamformer $\mathbf{f}$ of the transmitter, the the passive reflecting beamformer $\mathbf{\Phi}$ of the IRS and the energy combiner $\mathbf{w}$ of the EU, which is formulated as

$$\text{(P2)}: \max_{\mathbf{w},\mathbf{f},\mathbf{\Phi}} P_{RF} = ||\mathbf{w}^H (\mathbf{H}_d + \mathbf{G}\mathbf{\Phi}\mathbf{H}_r)\mathbf{f}||_2^2, \tag{6}$$

$$\text{s.t. } (5b), (5c), (5d)$$

Problem (P2) is difficult to solve, since both the energy combiner $\mathbf{w}$ and the passive reflecting beamformer $\mathbf{\Phi}$ of the IRS contains discrete variables, while they are coupled with the transmit beamformer $\mathbf{f}$. Moreover, the constraints (5b) and (5c) are non-convex. Two algorithms are proposed to solve (P2) in Section III and Section IV, respectively.

Moreover, the sub-problem (P3) maximises the output DC power by optimising the power splitter of the ER, which is detailed in Section V. The problem is formulated as

$$\text{(P3)}: \max_{\boldsymbol{\rho}} \sum_{j=1}^{N} \Psi(\boldsymbol{\rho}(j) P_{RF}) \tag{7}$$

$$\text{s.t. } (5e), (5f)$$

III. Successive Linear Approximation based Algorithm for solving (P2)

By relaxing the discrete constraints to the continuous ones, (P2) is then transformed as

$$\text{(P4)}: \max_{\mathbf{w}_c,\mathbf{f},\mathbf{\Phi}_c} ||\mathbf{w}_c^H(\mathbf{H}_d+\mathbf{G}\mathbf{\Phi}_c\mathbf{H}_r)\mathbf{f}||_2^2, \tag{8}$$

$$\text{s.t. } ||\mathbf{f}||_2^2 \le P_t, \tag{8a}$$

$$||\mathbf{w}_c(i)||_2^2 = 1,\ i=1,\cdots,N_r, \tag{8b}$$

$$||\mathbf{\Phi}_c(m,m)||_2^2 = 1,\ m=1,\cdots,M, \tag{8c}$$

where $\mathbf{w}_c$ and $\mathbf{\Phi}_c$ are both constituted by continuous phase-shifters.

We first optimise the passive reflecting beamformer, in Section III-A when given the transmit beamformer and the energy combiner. Then the the transmit beamformer and the energy combiner are obtained in Section III-B given a fixed passive reflecting beamformer. Finally, a successive linear approximation (SLA) based algorithm is proposed to jointly design the passive reflecting beamformer, the transmit beamformer and the energy combiner in Section III-C.

A. Passive Reflecting Beamformer design of the IRS

Given fixed $\mathbf{f}$ and $\mathbf{w}_c$, (P4) is reformulated as

$$\text{(P4.1)}: \max_{\mathbf{\Phi}_c} ||\mathbf{w}_c^H\mathbf{H}_d+\mathbf{w}_c^H\mathbf{G}\mathbf{\Phi}_c\mathbf{H}_r\mathbf{f}||_2^2, \tag{9}$$

$$\text{s.t. } ||\mathbf{\Phi}_c(m,m)||_2^2 = 1\ m=1,\cdots,M, \tag{9a}$$

By considering the unique structure of the diagonal matrix $\mathbf{\Phi}_c$, we have $\mathbf{w}_c^H\mathbf{G}\mathbf{\Phi}_c\mathbf{H}_r = \text{vec}(\mathbf{\Phi}_c)\ diag(\mathbf{w}_c^H\mathbf{G})\mathbf{H}_r$, where $\text{vec}(\mathbf{\Phi}_c) \in \mathbb{C}^{1\times M}$ is a vector converted by the diagonal element of the matrix $\mathbf{\Phi}_c$ and $diag(\mathbf{w}_c^H\mathbf{G}) \in \mathbb{C}^{M\times M}$ is the diagonal matrix generated by the vector $\mathbf{w}_c^H\mathbf{G}$. Letting $\mathbf{\Theta} = diag(\mathbf{w}_c^H\mathbf{G})\mathbf{H}_r\mathbf{f}$, (P4.1) can be then converted into

$$\text{(P4.1.1)}: \max_{\mathbf{\Phi}_c} \text{Re}\{\text{vec}(\mathbf{\Phi}_c)\mathbf{\Theta}\mathbf{\Theta}^H\text{vec}(\mathbf{\Phi}_c)^H + 2\mathbf{w}_c^H\mathbf{H}_d\mathbf{\Theta}^H\text{vec}(\mathbf{\Phi}_c)^H\}, \tag{10}$$

$$\text{s.t. } ||\text{vec}(\mathbf{\Phi}_c)(m)||_2^2 = 1,\ m=1,\cdots,M, \tag{10a}$$

However, problem (P4.1.1) is still non-convex. The minorize-maximisation (MM) [26], [27] technique is then relied upon for approximating the quadratic term in the objective function. We define an auxiliary function as

$$F(\text{vec}(\mathbf{\Phi}_c)|\text{vec}(\mathbf{\Phi}_c{}^{n-1})) = \text{Re}\{\text{vec}(\mathbf{\Phi}_c{}^{n-1})\mathbf{\Theta}\mathbf{\Theta}^H\text{vec}(\mathbf{\Phi}_c)^H + 2\mathbf{w}_c^H\mathbf{H}_d\mathbf{\Theta}^H\text{vec}(\mathbf{\Phi}_c)^H\} \tag{11}$$

where $\text{vec}(\mathbf{\Phi}_c{}^{n-1})$ is a given solution.The linear approximation of (P4.1.1) is then formulated as

$$\text{(P4.1.2)}: \max_{\mathbf{\Phi}_c^n} F(\text{vec}(\mathbf{\Phi}_c^n)|\text{vec}(\mathbf{\Phi}_c{}^{n-1})), \tag{12}$$

$$\text{s.t. } ||\text{vec}(\mathbf{\Phi}_c^n)(m)||_2^2 = 1\ m=1,\cdots,M, \tag{12a}$$

Denote $\text{vec}(\mathbf{\Phi}_c{}^n)$ as the optimal solution to (P4.1.2). We then have $F(\text{vec}(\mathbf{\Phi}_c{}^n)|\text{vec}(\mathbf{\Phi}_c{}^n)) \ge F(\text{vec}(\mathbf{\Phi}_c{}^n)|\text{vec}(\mathbf{\Phi}_c{}^{n-1})) \ge F(\text{vec}(\mathbf{\Phi}_c{}^{n-1})|\text{vec}(\mathbf{\Phi}_c{}^{n-1}))$. The detailed proof is given in Appendix A. Therefore, solving (P4.1.2) returns us a local optimum, which represents an sub-optimal lower-bound of (P4.1.1).

Unfortunately, (P4.1.2) is still non-convex due to the unity constrains (12a) on $\mathbf{\Phi}_c{}^n$. By relaxing these unity constraints, the following convex optimisation problem is obtained as

$$\text{(P4.1.3)}: \max_{\mathbf{\Phi}_c{}^n} F(\text{vec}(\mathbf{\Phi}_c)|\text{vec}(\mathbf{\Phi}_c{}^{n-1})), \tag{13}$$

$$\text{s.t. } ||\text{vec}(\mathbf{\Phi}_c{}^n)(m)||_2^2 \le 1\ m=1,\cdots,M. \tag{13a}$$

Proposition 1: The optimal solution to (P4.1.2) is exactly the same as that to (P4.1.3).

Proof: Please refer to Appendix B. ∎

Since (P4.1.3) is convex, the dual gap between the original problem and its dual counterpart is zero. Therefore, the optimal solution can be obtained by solving the dual problem. The Lagrangian function of (P4.1.3) is expressed as

$$L(\text{vec}(\mathbf{\Phi}_c{}^n),\boldsymbol{\lambda}) = \text{Re}\{(\text{vec}(\mathbf{\Phi}_c{}^{n-1}))\mathbf{\Theta}\mathbf{\Theta}^H\text{vec}(\mathbf{\Phi}_c{}^n)^H + 2\mathbf{w}_c^H\mathbf{H}_d\mathbf{\Theta}^H(\text{vec}\mathbf{\Phi}_c{}^n)^H\} + \sum_{i=1}^{M}\boldsymbol{\lambda}_i(\text{vec}(\mathbf{\Phi}_c{}^n)(m)(\text{vec}(\mathbf{\Phi}_c{}^n)(m))^H-1) \tag{14}$$

The dual function can be obtained by solving the following problem

$$g(\boldsymbol{\lambda}) \triangleq \max_{\text{vec}(\mathbf{\Phi}_c^n)} L(\text{vec}(\mathbf{\Phi}_c{}^n),\boldsymbol{\lambda}) \tag{15}$$

Then, the dual problem is formulated as

$$\text{(P4.1.4)}: \min_{\boldsymbol{\lambda}} g(\boldsymbol{\lambda}), \tag{16}$$

$$\text{s.t. } \boldsymbol{\lambda}(i) \ge 0\ i=1,\cdots,M \tag{16a}$$

The KKT condition on (P4.1.4) is expressed as

$$\begin{cases} \boldsymbol{\lambda}(i) \ge 0,\ i=1,\cdots,M \\ \boldsymbol{\lambda}(i)(\text{vec}(\mathbf{\Phi}_c{}^n)(i)(\text{vec}(\mathbf{\Phi}_c{}^n)(i))^H-1)=0,\ i=1,\cdots,M \\ \mathbf{a}(i)+\mathbf{b}(i)+\boldsymbol{\lambda}(i)\text{vec}(\mathbf{\Phi}_c)^{(n)}(i)=0,\ i=1,\cdots,M \end{cases} \tag{17}$$

where $\mathbf{a} = (\text{vec}(\mathbf{\Phi}_c{}^{n-1}))\mathbf{\Theta}\mathbf{\Theta}^H$ and $\mathbf{b} = 2\mathbf{w}_c^H\mathbf{H}_d\mathbf{\Theta}^H$. By solving Eq.(17), the i-th element in $\text{vec}(\mathbf{\Phi}_c{}^n)$ is expressed in close-form as

$$\text{vec}(\mathbf{\Phi}_c{}^n)(i) = (\mathbf{a}(i)+\mathbf{b}(i))^H/||\mathbf{a}(i)+\mathbf{b}(i)||. \tag{18}$$

Given fixed $\text{vec}(\mathbf{\Phi}_c{}^{n-1})$, we can obtain $\text{vec}(\mathbf{\Phi}_c{}^n)$ by Eq. (18). As a result, by initialising $\text{vec}(\mathbf{\Phi}_c{}^0)$, we may sequentially obtain $\text{vec}(\mathbf{\Phi}_c{}^0), \text{vec}(\mathbf{\Phi}_c{}^1), \cdots, \text{vec}(\mathbf{\Phi}_c{}^n), \cdots$. When n is sufficiently large, the objective of (P4.1.1) converges. The corresponding solution can be regarded as the sub-optimal solution $\text{vec}(\mathbf{\Phi}_c{}^*) = \text{vec}(\mathbf{\Phi}_c{}^n)$ to (P4.1). The main steps for solving (P4.1) is summarised as Algorithm 1.

Convergence Analysis: Since the the objective function is continuous and the constraints are continuous and in the closed interval, the optimum has a upper bound. During the $(n-1)$-th alteration, the objective value satisfies the following inequalities: $F(\text{vec}(\mathbf{\Phi}_c{}^{n-1})|\text{vec}(\mathbf{\Phi}_c{}^{n-1}) \ge F(\text{vec}(\mathbf{\Phi}_c{}^{n-1})|\text{vec}(\mathbf{\Phi}_c)^{n-2})$. Note that $F(\text{vec}(\mathbf{\Phi}_c{}^{n-1})|\text{vec}(\mathbf{\Phi}_c{}^{n-1})$ is the objective function of (P4.1), which also an upper-bound on the objective function of (P4.1.2) and (P4.1.3). We also have $F(\text{vec}(\mathbf{\Phi}_c{}^n)|\text{vec}(\mathbf{\Phi}_c{}^{n-1}) \ge F(\text{vec}(\mathbf{\Phi}_c{}^{n-1})|\text{vec}(\mathbf{\Phi}_c{}^{n-1})$. Therefore, the objective value of (P4.1.2) increases after every iteration. It will be convergent to a local optimal solution.

Algorithm 1 Phase-shifters of the IRS Design

Input: The channel $\mathbf{H}_d$, $\mathbf{H}_r$ and $\mathbf{G}$. Initialize the transmit beamformer $\mathbf{f}$, energy combiner $\mathbf{w}$ and the passive reflecting beamformer $\text{vec}(\mathbf{\Phi}_c{}^0)$ of the IRS; error tolerance ε; $F^1 = 0$; $n = 0$;

Output: The phase-shifter $\text{vec}(\mathbf{\Phi}_c)^*$ of the IRS;

1: **while** $(\delta > \varepsilon)$ **do**
2: $n \leftarrow n + 1$;
3: $F^0 \leftarrow F^1$;
4: Obtain the the phase-shifters $\text{vec}(\mathbf{\Phi}_c{}^n)$ of the IRS by substituting $\text{vec}(\mathbf{\Phi}_c{}^{n-1})$ into Eq. (18);
5: $F^1 \leftarrow F(\text{vec}(\mathbf{\Phi}_c{}^n)|\text{vec}(\mathbf{\Phi}_c{}^{n-1}))$;
6: $\delta \leftarrow ||F^1 - F^0||$;
7: **end while**
8: **return** $\text{vec}(\mathbf{\Phi}_c{}^*) \leftarrow \text{vec}(\mathbf{\Phi}_c{}^n)$.

Algorithm 2 Transmit Beamformer and Energy Combiner Design

Input: The channel $\mathbf{H}_d$, $\mathbf{H}_r$, $\mathbf{G}$ and the passive reflecting beamformer $\mathbf{\Phi}_c$ of the IRS. Initialize the energy combiner $\mathbf{w}_c{}^{n-1}$; error tolerance ε; $Q^1 = 0$; $n = 0$;

Output: The energy combiner $\mathbf{w}_c{}^*$, and the beamformer $\mathbf{f}^*$;

1: **while** $(\delta > \varepsilon)$ **do**
2: $n \leftarrow n + 1$;
3: $Q^0 \leftarrow Q^1$;
4: Obtain the energy combiner $\mathbf{w}_c{}^n$ by substituting $\mathbf{w}^{n-1}$ into Eq. (25);
5: $Q^1 \leftarrow Q(\mathbf{w}_c{}^n|\mathbf{w}_c{}^{n-1})$;
6: $\delta \leftarrow ||Q^1 - Q^0||$;
7: **end while**
8: Obtain the beamformer $\mathbf{f}^*$ by substituting $\mathbf{w}^n$ into Eq. (18);
9: **return** $\mathbf{w}_c{}^* \leftarrow \mathbf{w}_c{}^n$ and $\mathbf{f}^*$;

B. Transmit Beamformer and Energy Combiner Design

Given fixed continuous passive reflecting beamformer $\mathbf{\Phi}_c$ of the IRS, the problem (P3) is reformulated as

$$\text{(P4.2)}: \max_{\mathbf{w}_c,\mathbf{f}} ||\mathbf{w}_c^H(\mathbf{H}_d + \mathbf{G}\mathbf{\Phi}_c\mathbf{H}_r)\mathbf{f}||_2^2, \tag{19}$$

$$\text{s.t. } ||\mathbf{f}||_2^2 \le P_t, \tag{19a}$$

$$||\mathbf{w}_c(i)||_2^2 = 1 \ i = 1, \cdots, N_r, \tag{19b}$$

Given an arbitrary $\mathbf{w}_c$, $\mathbf{w}_c^H(\mathbf{H}_d + \mathbf{G}\mathbf{\Phi}_c\mathbf{H}_r)$ is a vector. Therefore, the optimal transmit beamformer is its conjugate vector, which is expressed as

$$\mathbf{f}^* = \sqrt{P_t}\frac{(\mathbf{H}_d + \mathbf{G}\mathbf{\Phi}_c\mathbf{H}_r)^H\mathbf{w}_c}{||\mathbf{w}_c^H(\mathbf{H}_d + \mathbf{G}\mathbf{\Phi}_c\mathbf{H}_r)||} \tag{20}$$

By substituting Eq. (20) into the objective function (19) of (P4.2), (P4.2) is reformulated as

$$\text{(P4.2.1)}: \max_{\mathbf{w}_c} ||\mathbf{w}_c^H(\mathbf{H}_d + \mathbf{G}\mathbf{\Phi}_c\mathbf{H}_r)(\mathbf{H}_d + \mathbf{G}\mathbf{\Phi}_c\mathbf{H}_r)^H\mathbf{w}_c||_2^2, \tag{21}$$

$$\text{s.t. } ||\mathbf{w}_c(i)||_2^2 = 1 \ i = 1, \cdots, N_r, \tag{21b}$$

Similarly to (P4.1), the MM method is also adopted for solving (P4.2.1), while the constraints (21b) are relaxed to their convex counterparts. By defining $Q(\mathbf{w}_c{}^n|\mathbf{w}_c{}^{n-1}) = \text{Re}\{(\mathbf{w}_c{}^{n-1})^H(\mathbf{H}_d + \mathbf{G}\mathbf{\Phi}_c\mathbf{H}_r)(\mathbf{H}_d + \mathbf{G}\mathbf{\Phi}_c\mathbf{H}_r)^H\mathbf{w}_c{}^n\}$. The linear approximation of (P4.2.1) is reformulated as

$$\text{(P4.2.2)}: \max_{\mathbf{w}_c{}^n} Q(\mathbf{w}_c{}^n|\mathbf{w}_c{}^{n-1}) \tag{22}$$

$$\text{s.t. } ||\mathbf{w}_c{}^n(i)||_2^2 \le 1 \ i = 1, \cdots, N_r, \tag{22b}$$

Similar to *Proposition 1*, (P4.2.2) also shares the same optimal solution with (P4.3.1). Since (P4.2.2) is convex, its Lagrangian function is expressed as

$$L(\mathbf{w}_c{}^n, \boldsymbol{\mu}) = \boldsymbol{\beta}\mathbf{w}_c{}^n + \sum_{i=1}^{N_r}\boldsymbol{\mu}(i)(\mathbf{w}_c{}^n(\mathbf{w}_c{}^n)^H - 1). \tag{23}$$

where $\boldsymbol{\beta} = (\mathbf{w}_c{}^{n-1})^H(\mathbf{H}_d + \mathbf{G}\mathbf{\Phi}_c\mathbf{H}_r)(\mathbf{H}_d + \mathbf{G}\mathbf{\Phi}_c\mathbf{H}_r)^H$. The corresponding KKT condition is derived as

$$\begin{cases} \boldsymbol{\mu}(i) \ge 0, \ i = 1, 2, \cdots, M, \\ \boldsymbol{\mu}(i)(\mathbf{w}_c{}^n(i)(\mathbf{w}_c{}^n(i))^H - 1) = 0, \ i = 1, 2, \cdots, N_r, \\ \boldsymbol{\beta}(i)^H + \boldsymbol{\mu}(i)\mathbf{w}_c{}^n(i) = 0, \ i = 1, 2, \cdots, N_r. \end{cases} \tag{24}$$

By solving Eq. (24), the i-th element of the optimal energy combiner $\mathbf{w}_c{}^n$ is expressed in close-form as

$$\mathbf{w}_c{}^n(i) = \boldsymbol{\beta}(i)^H/||\boldsymbol{\beta}(i)||. \tag{25}$$

Algorithm 2 is then summarised for solving (P4.2)

Convergence Analysis: Since the the objective function is continuous and the constraints are continuous and in the closed interval, the optimum has a upper bound. During the n-th alteration, the objective value satisfies the following inequalities: $Q(\mathbf{w}_c{}^n|\mathbf{w}_c{}^{n-1}) \ge Q(\mathbf{w}_c{}^{n-1}|\mathbf{w}_c{}^{n-1}) \ge Q(\mathbf{w}_c{}^{n-1}|\mathbf{w}_c{}^{n-2})$. Therefore, the objective value of (P4.2) increases after every iteration. It will converse to a local optimum.

C. Joint Design

With the aid of Algorithm 1 and Algorithm 2, we may obtain the continuous energy combiner $\mathbf{w}_c$ of the ER and the the passive reflecting beamformer $\mathbf{\Phi}_c$ of the IRS. Their optimal discrete solution can be obtained as

$$\begin{aligned} \mathbf{w}^*(i) &= \arg\min_{\mathbf{w}(i)} ||\mathbf{w}(i) - \mathbf{w}_c^*(i)||, \\ \mathbf{\Phi}^*(i) &= \arg\min_{\mathbf{\Phi}(m,m)} ||\mathbf{\Phi}(i) - \mathbf{\Phi}_c^*(m,m)||, \end{aligned} \tag{26}$$

which can be solved by a one-dimension exhaustive search.

Finally, SLA based joint design for solving (P2) is detailed in Algorithm 3. Algorithm 3 has two loops. Given any energy combiner, we optimise the passive reflecting beamformer by solving (P4.1) and the energy combiner is obtained by solving (P4.2) with a given passive reflecting beamformer in the outer loop. Moreover, we linearly approximate the original objective functions of (P4.1) and (4.2) to linear peers. (P4.1) and (P4.2) are successively solved in the inner-loop.

Complexity Analysis: The total complexity is $O([Ml_1 + N_rM(N_r + N_t)l_2]l_3)$, where l_1, l_2 and l_2 are the number of iterations in Algorithm 1, 2 and 3, respectively. Based on our numerical result, the number of the iterations in our algorithm is 4, which is much lower than that of [20].

Convergence Analysis: The continuous solution in Algorithm 3 converses to the KKT point. Please refer to Appendix C for more details.

Algorithm 3 SLA algorithm

Input: The channel $\mathbf{H}_d$, $\mathbf{H}_r$ and $\mathbf{G}$. Initialize energy combiner ${\mathbf{w}_c}^0$ and beamformer $\mathbf{f}^0$; error tolerance ε; $F^1 = 0$; $n = 0$;
Output: The energy combiner $\mathbf{w}^*$, the phase of IRS $\mathbf{\Phi}^*$ and the beamformer $\mathbf{f}^*$;
1: **while** $(\delta > \varepsilon)$ **do**
2: $n \leftarrow n + 1$;
3: $F^0 \leftarrow F^1$;
4: Obtain the continues phase of IRS ${\mathbf{\Phi}_c}^n$ by substituting ${\mathbf{w}_c}^{(n-1)}$ and $\mathbf{f}^{(n-1)}$ into Algorithm 1;
5: Obtain the continues energy combiner ${\mathbf{w}_c}^n$ and beamformer $\mathbf{f}^n$ by substituting ${\mathbf{\Phi}_c}^n$ into Algorithm 2;
6: $F^1 \leftarrow ||({\mathbf{w}_c}^n)^H(\mathbf{H}_d + \mathbf{G}{\mathbf{\Phi}_c}^n\mathbf{H}_r)\mathbf{f}^n||_2^2$
7: $\delta \leftarrow ||F^1 - F^0||$;
8: **end while**
9: Obtain the discrete energy combiner $\mathbf{w}^*$ and the discrete phase of IRS $\mathbf{\Phi}^*$ by Eq. (26);
10: Obtain the beamformer $\mathbf{f}^*$ by Eq.(18)
11: **return** $\{\mathbf{f}^*, \mathbf{w}^*$ and $\mathbf{\Phi}^*\}$;

IV. Quadratic Assignment Program based Solution to (P2)

Through we derive the close-form solution in the SLA based algorithm, the attained WPT performance is compromised due to the relaxation of the objective function. Then, we propose an improved greedy randomized adaptive search procedure (I-GRASP) to directly solve (P2).

For any given energy combiner $\mathbf{w}$ and passive reflecting beamformer $\mathbf{\Phi}$, the optimal transmit beamformer is obtained by the maximum ratio transmitting, which is expressed as $\mathbf{f}^* = \sqrt{P_t}(\mathbf{H}_d + \mathbf{G}\mathbf{\Phi}\mathbf{H}_r)^H\mathbf{w}$. Therefore, when $\mathbf{w}$ is given, (P2) is reformulated as

$$\text{(P5.1)}: \max_{\mathbf{\Phi}} \ \mathbf{w}^H(\mathbf{H}_d + \mathbf{G}\mathbf{\Phi}\mathbf{H}_r)(\mathbf{H}_d + \mathbf{G}\mathbf{\Phi}\mathbf{H}_r)^H\mathbf{w}, \quad (27)$$

$$\text{s.t. } \mathbf{\Phi}(m,m) \in \mathcal{F}, \ m = 1, \cdots, M, \quad (27c)$$

We convert (P5.1) to a standard 0-1 QAP problem, which requires that the objective function is minimised and the coefficients of quadratic terms are positive. The QAP programming has been widely investigated in combination optimisation [28]–[30], which could be solved by classic and advanced algorithms such as branch-and-bound method and GRASP, respectively.

Define a binary vector $\mathbf{x}_m \in R^{l\times 1}$ with at most one element being non-zero, where $\mathbf{x}_m$ satisfies $\sum_{i=1}^{l}\mathbf{x}_m(i) = 1$ and $l = 2^b$, while b represents the resolution of phase-shifter. The m-th reflector in the IRS is expressed as $\mathbf{\Phi}(m,m) = \boldsymbol{\phi}^H\mathbf{x}_m$, where we have $\boldsymbol{\phi} = [1, e^{j2\pi/l}, \cdots, e^{j(l-1)2\pi/l}]^H$. By letting the vector $\mathbf{x} = [\mathbf{x}_1; \cdots; \mathbf{x}_M]$ of the size $lM \times 1$, the passive reflecting beamformer is reformulated as $\mathbf{\Phi} = \text{diag}((\mathbf{I}_M \otimes \boldsymbol{\phi})\mathbf{x})$. As a result, (P5.1) is reformulated as

$$\text{(P5.2)}: \max_{\mathbf{x}} \ \mathbf{x}^H\mathbf{Q}\mathbf{x} + 2\Re\{\mathbf{x}^H\mathbf{T}\}, \quad (28)$$

$$\text{s.t. } \mathbf{x}_m = 1, \forall m. \quad (28a)$$

where $\mathbf{Q} = (diag(\mathbf{w}^H\mathbf{G})\mathbf{H}_r\mathbf{H}_r^H diag(\mathbf{w}^H\mathbf{G})^H) \otimes (\boldsymbol{\phi}\boldsymbol{\phi}^H)$ and $\mathbf{T} = vec(\boldsymbol{\phi}\mathbf{w}^H\mathbf{H}_d diag(\mathbf{w}^H\mathbf{G})\mathbf{H}_r)$.

However, (P5.2) is not a standard QAP problem, since it does not minimise the objective function and $\mathbf{Q}$ in Eq. (28) is not a real positive matrix. The objective function of (P5.2) can be then reformulated as

$$\begin{aligned}&\max_{\mathbf{x}} \ \mathbf{x}^H\mathbf{Q}\mathbf{x} + 2\Re\{\mathbf{x}^H\mathbf{T}\}\\ &= \min_{\mathbf{x}} \ -\mathbf{x}^H\Re\{\mathbf{Q}\}\mathbf{x} - 2\mathbf{x}^H\Re\{\mathbf{T}\}\\ &= \min_{\mathbf{x}} \ \mathbf{x}^H\mathbf{Q}_1\mathbf{x} - 2\mathbf{x}^H\Re\{\mathbf{T}\} \quad (29)\end{aligned}$$

where we have $\mathbf{Q}_1 = k\mathbf{E} - \Re\{\mathbf{Q}\}$ and $k > \max(\Re\{\mathbf{Q}\})$. Note that the constant $k\mathbf{x}^H\mathbf{I}\mathbf{x}$ is a constant number, which can be ignored in Eq. (29). Therefore, (P5.2) can be equivalently reformulated as

$$\text{(P5.3)}: \min_{\mathbf{x}} \ \mathbf{x}^H\mathbf{Q}_1\mathbf{x} - 2\mathbf{x}^H\Re\{\mathbf{T}\}, \quad (30)$$

$$\text{s.t. } \sum_{i=1}^{l}\mathbf{x}_m(i) = 1, \forall m. \quad (30a)$$

Now, (P5.3) is a standard QAP problem.

The I-GRASP based joint design for solving (P2) is detailed in Algorithm 3. The main idea of I-GRASP is to choose the best solution from all the iterations, while a greedy randomized solution is initialised in every iteration for rapidly achieving the local optimum. The main steps are summarized as below:

1) Greedy randomized solution: The details are shown in line 2-9 in the Algorithm 3. We first obtain (P5.2) by randomly initializing the energy combiner $\mathbf{w}$ and set $\mathbf{x} = 0$. We randomly choose the i-th element $\mathbf{x}_i$ in $\mathbf{x}$ and obtain $\mathbf{x}_i$ by solving (P5.4), which is expressed as

$$\text{(P5.4)}: \min_{\mathbf{x}_i} \ \mathbf{x}^H\mathbf{Q}_1\mathbf{x} - 2\mathbf{x}^H\Re\{\mathbf{T}\}, \quad (31)$$

$$\text{s.t. } \sum_{j=1}^{l}\mathbf{x}_i(j) = 1. \quad (31a)$$

Then we repeat the following process until $\mathbf{x}_i$, for $\forall\ i = 1, 2, \cdots, M$ are optimised. By updating the i-the element $\mathbf{x}_i$ in $\mathbf{x}$, the restricted candidate list (RCL) of unoptimised elements in $\mathbf{x}$ is expressed as

$$RCL = sort\left[\frac{\partial(\mathbf{x}^H\mathbf{Q}_1\mathbf{x} - 2\mathbf{x}^H\Re\{\mathbf{T}\})}{\partial\mathbf{x}_1}, \cdots, \frac{\partial(\mathbf{x}^H\mathbf{Q}_1\mathbf{x} - 2\mathbf{x}^H\Re\{\mathbf{T}\})}{\partial\mathbf{x}_M}\right], \quad (32)$$

where the function $sort(\cdot)$ arranges the partial derivatives from large ones to small. RCL evaluates the impact of each element on the objective function. By defining the greedy factor g satisfying $1 \le g \le M$, we generate a random number k from the set $\{1, \cdots, g\}$. We then select the k-th element $\mathbf{x}_k$ at the RCL and obtain $\mathbf{x}_k$ by solving (P5.4).

2) Local search: The details are shown in line 11-18 in the Algorithm 3. The matrix x can be expressed as the following partitioned form

$$\mathbf{x} = [\underbrace{\mathbf{x}_1, \cdots, \mathbf{x}_i}_{\mathbf{x}^{(1)}}, \underbrace{\mathbf{x}_{i+1}, \cdots, \mathbf{x}_{i+k}}_{\mathbf{x}^{(2)}}, \underbrace{\mathbf{x}_{i+k+1}, \cdots, \mathbf{x}_M}_{\mathbf{x}^{(3)}}], \quad \forall i = 1, \cdots, M/k. \quad (33)$$

Then, with the same value of i, the corresponding partitioned format of matrices $\mathbf{T}$ and $\mathbf{Q}_1$ are

Algorithm 4 I-GRASP Algorithm

Input: The channel $\mathbf{H}_d$, $\mathbf{H}_r$ and $\mathbf{G}$, the number of iterations N, the size of block k, the greedy factor g;
Output: The energy combiner $\mathbf{w}^*$, the phase of IRS $\mathbf{\Phi}^*$ and the beamformer $\mathbf{f}^*$;

```
for n = 1 : N do
    Obtain (P5.2) by randomly initialize energy combiner w; Set x = 0;
    Randomly choose the i-th reflector; Obtain x_i by maximising (P5.4).
    for m = 1 : M and m ≠ i do
        Make the restricted candidate list (RCL) by Eq. (32);
        Randomly choose number r from the set [1, 2, ··· , g];
        Select the element x_r at the RCL.
        Obtain the x_i by maximising (P5.4).
    end for
    repeat
        for i = 1 : M/k do
            Update x_i, ··· , x_{i+k} by Eq. (37).
        end for
        for j = 1 : N_r do
            w_i = arg max(w(i)h_i w + w(i)^H h_i^H w^H);
        end for
    until x stays constant
end for
Choose the solution with the highest performance and convert to Φ* and w*
Obtain f by f* = sqrt(P_t)(H_d + GΦ*H_r)^H w*.
return {f*, w* and Φ*};
```

expressed as $\mathbf{T} = [\mathbf{T}^{(1)}, \mathbf{T}^{(2)}, \mathbf{T}^{(3)}]$ and $\mathbf{Q}_1 = [\mathbf{Q}_1^{(11)}, \mathbf{Q}_1^{(12)}, \mathbf{Q}_1^{(13)}; \mathbf{Q}_1^{(21)}, \mathbf{Q}_1^{(22)}, \mathbf{Q}_1^{(23)}; \mathbf{Q}_1^{(31)}, \mathbf{Q}_1^{(32)}, \mathbf{Q}_1^{(33)}]$, respectively. Given $\mathbf{x}^{(1)}$ and $\mathbf{x}^{(3)}$, (P5.3) is reformulated as

$$\text{(P5.5)}: \min_{\mathbf{x}^{(2)}} \mathbf{x}^H \mathbf{Q}_1 \mathbf{x} - 2\mathbf{x}^H \Re\{\mathbf{T}\} = \mathbf{S}_i + \mathbf{x}^{(2)} \mathbf{R}_i, \quad (34)$$

$$\text{s.t.} \sum_{i=1}^{l} \mathbf{x}_m(i) = 1, \forall m = i, \cdots, i+k. \quad (34a)$$

where we have

$$\mathbf{S}_i = \sum_{i=1}^{Ml} \mathbf{Q}_1(i,i) + 2\mathbf{x}^{(1)^H} \mathbf{Q}_1^{(31)} \mathbf{x}^{(3)} - 2\mathbf{x}^{(1)^H} \mathbf{T}^{(1)} - 2\mathbf{x}^{(3)^H} \mathbf{T}^{(3)}; \quad (35)$$

$$\mathbf{R}_i = 2\mathbf{Q}_1^{(21)} \mathbf{x}^{(1)} + 2\mathbf{Q}_1^{(23)} \mathbf{x}^{(3)} - \mathbf{T}^{(2)}. \quad (36)$$

The optimal solution to (P5.5) is then expressed as

$$\mathbf{x}^{(2)} = \arg\max(\mathbf{S}_i + \mathbf{x}^{(2)} \mathbf{R}_i), \quad (37)$$

which can be obtained by exhaustive search.

The local optimal solution of the i-th element in energy combiner $\mathbf{w}$ is updated by

$$\mathbf{w}(i) = \arg\max(\mathbf{w}(i)\mathbf{h}_i \mathbf{w} + \mathbf{w}(i)^H \mathbf{h}_i^H \mathbf{w}^H), \quad (38)$$

where we have $[\mathbf{h}_1, \cdots, \mathbf{h}_M] = (\mathbf{H}_d + \mathbf{G}\mathbf{\Phi}\mathbf{H}_r)(\mathbf{H}_d + \mathbf{G}\mathbf{\Phi}\mathbf{H}_r)^H$.

Complexity Analysis: The complexity of I-GRASP is expressed as $\mathcal{O}(I(M^2 + k^2 M^3))$, where I is the number of iterations and k is the size of a block in the local search stage.

V. Design of Power Splitter Ratio

We then focus on (P4) in order to optimise the power splitter. We first consider a special case where the ER has two $N = 2$ energy harvesters. Let us define the function $f_2(\rho) = \Psi(\rho P_{RF}) + \Psi((1-\rho)P_{RF})$. The maximum value of $f_2(\rho)$ is obtained either at the extreme points or at the boundary points. The derivative of $f_2(\rho)$ with respect to ρ is expressed as

$$f_2'(\rho) = \frac{-MXaP_{RF}\exp(-a(\rho P_{RF} - b))}{[X + X\exp(-a(\rho P_{RF} - b))]^2} + \frac{MXaP_{RF}\exp(-a((1-\rho)P_{RF} - b))}{[X + X\exp(-a((1-\rho)P_{RF} - b))]^2}. \quad (39)$$

By letting $f_2'(\rho) = 0$, we obtain the unique extreme point $\rho^* = 0.5$. The optimal solution of (P2) is then expressed as

$$P_{out} = \max(\Psi(P_{RF}), 2\Psi(0.5P_{RF})). \quad (40)$$

Therefore, the optimal power splitting policy can be summarised as: If $\Psi(P_{RF}) \geq 2\Psi(0.5P_{RF})$, we have $\rho = 0$ or $\rho = 1$; If $\Psi(P_{RF}) < 2\Psi(0.5P_{RF})$, the uniform power splitter with $\rho = 0.5$ is optimal.

Let $\boldsymbol{\rho} = [\boldsymbol{\rho}(1), \boldsymbol{\rho}(2), \cdots, \boldsymbol{\rho}(N)]$ represents the corresponding portions of the RF energy flowing into different energy harvester, while satisfying $\sum_{j=1}^{N} \boldsymbol{\rho}(j) = 1$. Then, the function of the total DC power harvested is expressed as $f_N(\boldsymbol{\rho}) = \Psi(\boldsymbol{\rho}(1)P_{RF}) + \Psi(\boldsymbol{\rho}(2)P_{RF}), \cdots, \Psi(\boldsymbol{\rho}(N-1)P_{RF}) + \Psi((1 - \sum_{j=1}^{N-1} \boldsymbol{\rho}(j))P_{RF})$. The maximum of $f_N(\boldsymbol{\rho})$ is either an extreme point or a boundary point. We first consider the case of the extreme point. The partial derivatives of $f_N(\boldsymbol{\rho})$ are obtained as

$$\frac{\partial f_N}{\partial \boldsymbol{\rho}(j)} = \frac{-MaP_{RF}\exp(-a(\boldsymbol{\rho}(j)P_{RF} - b))}{X[1 + \exp(-a(\boldsymbol{\rho}(j)P_{RF} - b))]^2} + \frac{MaP_{RF}\exp(-a((1 - \sum_{i=1}^{N-1} \boldsymbol{\rho}(i))P_{RF} - b))}{X[1 + \exp(-a((1 - \sum_{i=1}^{N-1} \boldsymbol{\rho}(i))P_{RF} - b))]^2}, \quad (41)$$

for $j = 1, 2, ..., N-1$. By letting $\frac{\partial f_N}{\partial \boldsymbol{\rho}(j)} = 0$, we obtain the extreme point $\boldsymbol{\rho}^*(j) = 1/N$ for $\forall j = 1, 2, ..., N-1$. Next, we consider the boundary point of $f_N(\boldsymbol{\rho})$, which represents the case that $(N-1)$ energy harvester actually used. Therefore, we have $\boldsymbol{\rho}(N) = 0$. As a result, the maximum value achieved by this boundary point is equivalent to the maximum when $(N-1)$ energy harvesters are implemented in total at the energy receiver. This is also either from the extreme point or the boundary point, where the extreme point is $\boldsymbol{\rho}(k) = 1/(N-1)$ for $\forall k = 1, 2, \cdots, N-2$, while the boundary point is the energy receiver having $(N-2)$ energy harvester. As a result, the maximum output DC power is expressed as

$$P_{out} = \max(\Psi(P_{RF}), 2\Psi(0.5P_{RF}), \cdots, N\Psi(1/N \times P_{RF})). \quad (42)$$

Proposition 2: When $N \to \infty$, the extreme value of $f_N(\boldsymbol{\rho})$ is saturated.

Proof: Please refer Appendix D. ■

According to Eq. (42), the maximum output DC power with N energy harvesters is the maximum extreme value among $\{f_1, f_2, \cdots f_N\}$. Base on *Proposition* 2, the extreme value of f_N is saturated when N is sufficiently large. Therefore, we can

This article has been accepted for publication in IEEE Transactions on Wireless Communications. This is the author's version which has not been fully edited and content may change prior to final publication. Citation information: DOI 10.1109/TWC.2023.3251743

implement limited number of the energy harvesters before the output DC power saturates in order to maintain high hardware efficiency.

VI. Numerical Result

The transmitter is equipped with $N_t = 4$ antennas, while the receiver is equipped with $N_r = 3$ antennas. The number of reflectors in the IRS is $M = 100$. The distances form the transmitter to the IRS and to the ER are 1m and 5.5m, respectively, while the distance form the IRS to the ER is 5m. The path loss is modelled in dB as $PL = PL_0 - 10\alpha \log(d/d_0)$, where PL_0 is the path loss at the reference distance d_0, d denotes the signal propagation distance, and α represents the path loss exponent. We set $d_0 = 1$ and $PL_0 = -30$ dB. The pass loss exponent of the transmitter-IRS-EU link and the transmitter-EU link are set as $\alpha = 2.2$ and $\alpha = 3.6$ [17], respectively. The transmit antenna gain is set to 15 dBi [31]. The ER is equipped with a single or a pair of energy harvesters (Rec) where the optimal power splitter is adopted. The transmitter power is set to $P_t = 42$ dBm. We assume the same resolution for the phase-shifters of the IRS and those of the ER. For the non-linear energy harvester model of Eq. (4), we set $M = 24$ mW as the maximum DC power that could be output by a single energy harvester. Moreover, we set $a = 150$ and $b = 0.0022$ [7]. The insertion loss in the energy combing is set to 1.2 dB [32]

We assume a 2-D linear antenna array at both the transmitter and ER and a linear reflector array at the IRS. The IRS is connected to the transmitter and controlled by it. We assume that the direct channel $\mathbf{H}_d$ between the transmitter and the ER follows Rayleigh block fading without a clear line-of-sight (LOS) path. The channel coefficient $\mathbf{H}_d(i,j)$ satisfies $\mathbf{H}_d(i,j) \sim \mathcal{CN}(0,1)$ for $\forall i$, and $\forall j$. For the IRS related channels, i.e., $\mathbf{H}_r$ and $\mathbf{G}$, they both obey Rician block fading. For example, The 2D array channel model [R6] $\mathbf{H}_r$ between the transmitter and the IRS is written as

$$\mathbf{H}_r = \sqrt{\frac{\beta}{\beta+1}}\mathbf{H}_r{}^{LOS} + \sqrt{\frac{1}{\beta+1}}\mathbf{H}_r{}^{NLOS} \tag{43}$$

where β is the Rician factor, $\mathbf{H}_r{}^{LOS}$ is the deterministic LOS portion and $\mathbf{H}_r{}^{NLOS}$ is the non-LOS (NLOS) portion.

The LOS portion $\mathbf{H}_r{}^{LOS}$ can be further expressed as $\mathbf{H}_r{}^{LOS} = \mathbf{a}_r(\theta_2,\theta_1)^H\mathbf{a}_t(\theta_4,\theta_3)$. Assume that the IRS are equipped with a 2D uniform rectangular array in the xy-plane with M_1 and M_2 elements on the x and y axes, respectively. The arrival steering vector $\mathbf{a}_r(\theta_2,\theta_1)$ of this 2D array is obtained as $\mathbf{a}_r(\theta_2,\theta_1) = \mathbf{a}_{az}(\theta_2,\theta_1) \otimes \mathbf{a}_{el}(\theta_2,\theta_1)$, where θ_2 and θ_1 are the azimuth and elevation angles, respectively, while $\otimes$ represents the Kronecker product. Moreover, $\mathbf{a}_{az}(\theta_2,\theta_1) \in \mathbb{C}^{M_1\times 1}$ and $\mathbf{a}_{el}(\theta_2,\theta_1) \in \mathbb{C}^{M_2\times 1}$ are the uniform linear array steering vector expressed as

$$[\mathbf{a}_{az}(\theta_2,\theta_1)](n) = e^{-j(n-1)\frac{2\pi}{\lambda}d_2 sin(\theta_2)cos(\theta_1)}, \tag{44}$$

$$[\mathbf{a}_{el}(\theta_2,\theta_1)](n) = e^{-j(n-1)\frac{2\pi}{\lambda}d_2 sin(\theta_2)cos(\theta_1)}, \tag{45}$$

where λ is the wavelength, d_1 is the distance between two adjacent antennas. The departure steering vector $\mathbf{a}_t(\theta_4,\theta_3)$ has the same form as $\mathbf{a}_r(\theta_2,\theta_1)$, where θ_3 and θ_4 represent the azimuth and elevation angles, respectively. The spatial correlated NOLS portion is expressed as $\mathbf{H}^{NLOS} = \sum_{l=1}^{L}\alpha_l\mathbf{a}_r(\theta_l^{r_1},\theta_l^{r_2})\mathbf{a}_t(\theta_l^{t_1},\theta_l^{t_2})$, where L is the number of multi-paths, while α_l is the complex gain of l-th path. $\mathbf{a}_r$ and $\mathbf{a}_t$ represent the normalized receive and transmit array response vectors. Moreover, the wireless channel $\mathbf{G}$ from the IRS to the energy receiver has a similar form as $\mathbf{H}_r$. Araujo *et al* [33] designed the channel estimation for the IRS aided MIMO system by exploiting tensor modeling approach, while the uplink pilot transmission power is around -40 dBm [34].

A. Comparison with Different Algorithms

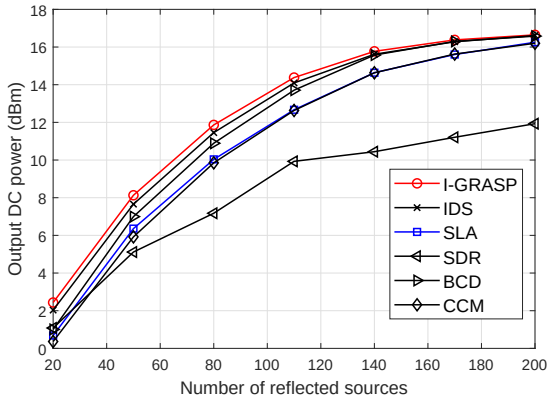

Fig. 2. Output DC power of three Algorithms.

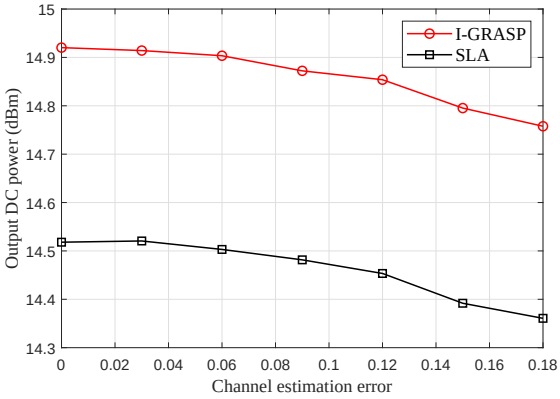

Fig. 3. Robust analysis.

We evaluate the output DC power on the number of reflectors with six different algorithms, namely I-GRASP, iterative discrete search (IDS), SLA, SDR [24], BCD [25] and CCM [25]. Note that IDS based algorithm was widely adopted in [20], [21]. Observe from Fig. 2 that our proposed I-GRASP in Section IV has the highest output DC power, comparing to the other counterparts.Our I-GRASP algorithm outperforms the IDS algorithm. This is because we generate a greedy randomized solution as the initialised solution in every iteration. Our I-GRASP algorithm has higher output DC power than the BCD, CCM and SDR based counterparts. This is because I-GRASP algorithm directly solve the discrete optimisation, while there is performance loss by recovering the discrete solution from the continuous counterpart with the

This article has been accepted for publication in IEEE Transactions on Wireless Communications. This is the author's version which has not been fully edited and content may change prior to final publication. Citation information: DOI 10.1109/TWC.2023.3251743

TABLE I
COMPLEXITY OF SIX ALGORITHMS

I-GRASP	IDS	SLA	SDR	BCD	CCM
$\mathcal{O}(I(M^3))$	$\mathcal{O}(M^3)$	$O(M)$	$\mathcal{O}(M^7)$	$\mathcal{O}(M^3)$	$\mathcal{O}(M^3)$

BCD, CCM and SDR based algorithms. Our SLA algorithm achieves almost the same WPT performance as the I-GRASP, IDS, BCD and CCM based algorithms. It substantially outperforms SDR based counterparts when the IRS has a large number of reflectors. This is because the SDR based algorithm cannot recover a good passive beamformer to achieve high performance with a limited number of randomizations in a high dimension space. We find that when the IRS only has 20 reflectors, the SDR based algorithm outperforms the CCM, BCD, and SLA based algorithms. Moreover, our proposed SLA algorithm in Section III-C has the lowest complexity as summarised in TABLE I, which demonstrates its advantage in practical implementations. Furthermore, as the number of reflectors in the IRS increases, the output DC power also increases until it saturates.

We investigate the impact of imperfect channel state information (CSI) in the channels on the WPT performance of our proposed algorithms. The channel estimation errors are modelled as

$$\mathbf{H}_r = \hat{\mathbf{H}}_r + \Delta_1, \quad \mathbf{G} = \hat{\mathbf{G}} + \Delta_2, \quad \mathbf{H}_d = \hat{\mathbf{H}}_d + \Delta_3, \quad (46)$$

where $\hat{\mathbf{H}}_r$, $\hat{\mathbf{G}}$ and $\mathbf{H}_d$ are the estimated channel coefficients from the transmitter to the IRS, those from the IRS to the ER and those from the transmitter to the ER, respectively. Δ_1, Δ_2 and Δ_3 are the channel estimated errors, which are independent to the $\hat{\mathbf{H}}_r$, $\hat{\mathbf{G}}$ and $\hat{\mathbf{H}}_d$, respectively. The solution obtained by imperfect CSI is denoted as $\{\hat{\mathbf{f}}, \hat{\mathbf{\Phi}}\ \hat{\mathbf{w}}\}$. The lower bound of the received RF power is expressed as

$$\begin{aligned} P_{RF} &= ||\hat{\mathbf{w}}(\mathbf{H}_d + \hat{\mathbf{G}}\hat{\mathbf{\Phi}}\hat{\mathbf{H}}_r)\hat{\mathbf{f}} + \hat{\mathbf{w}}\Delta_1\hat{\mathbf{\Phi}}\hat{\mathbf{H}}_r\hat{\mathbf{f}} + \hat{\mathbf{w}}\hat{\mathbf{G}}\hat{\mathbf{\Phi}}\Delta_2\hat{\mathbf{f}} \\ &+ \hat{\mathbf{w}}\Delta_1\hat{\mathbf{\Phi}}\Delta_2\hat{\mathbf{f}}||_2^2 \qquad (47) \\ &\geq \Big|\Big|||\hat{\mathbf{w}}(\hat{\mathbf{H}}_d + \hat{\mathbf{G}}\hat{\mathbf{\Phi}}\hat{\mathbf{H}}_r)\hat{\mathbf{f}}|| - ||\hat{\mathbf{w}}\Delta_1\hat{\mathbf{\Phi}}\hat{\mathbf{H}}_r\hat{\mathbf{f}}|| - ||\hat{\mathbf{w}}\hat{\mathbf{G}}\hat{\mathbf{\Phi}}\Delta_2\hat{\mathbf{f}}|| \\ &- ||\hat{\mathbf{w}}\Delta_1\hat{\mathbf{\Phi}}\Delta_2\hat{\mathbf{f}}|| - ||\hat{\mathbf{w}}\Delta_3\hat{\mathbf{f}}||\Big|\Big|_2^2. \end{aligned}$$

Eq. (47) indicates that the lower bound of the received RF power P_{RF} reduces with higher channel estimation errors.

The channel estimation error ratio is then set as $\delta = ||\Delta_1||/||\mathbf{H}_r||$. Moreover, we assume that the channel estimation error ratios are the same in the channel from the transmitter to the IRS, that from the IRS to the ER and that from the transmitter to the ER. Observe from Fig. 3 that the output DC power is highest with perfect CSI ($\delta = 0$). Furthermore, the output DC power reduces as we increase the channel estimation errors ratio, while the I-GRASP also outperforms the SLA counterpart.

Observe from both Figs. 2 and 3 that the performance gap between the I-GRASP and the SLA based algorithms is very small. Due to tits implementation advantage, the WPT performance of our IRS aided WPT system is then evaluated with the SLA based algorithm.

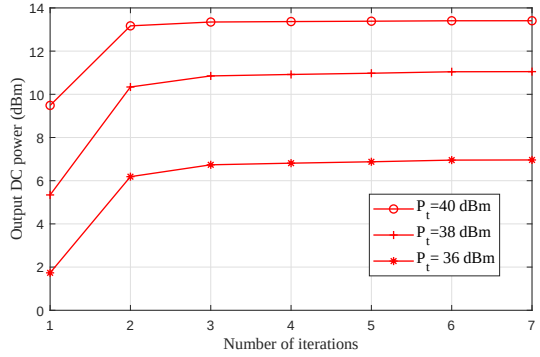

Fig. 4. Iteration vs output power when $N_t = 4$,$N_r = 3$,$M = 100$.

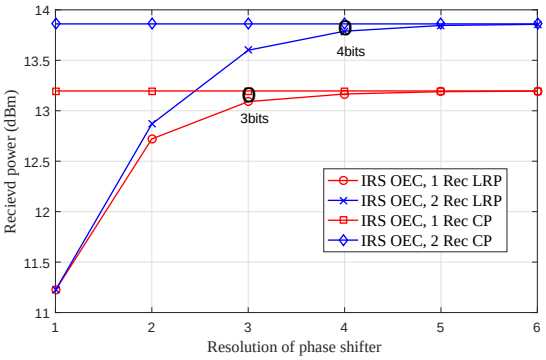

Fig. 5. Resolution of phase-shifter vs output power when $N_t = 4$,$N_r = 3$,$M = 100$.

B. The Impact of the IRS

We demonstrate the convergence of the proposed SLA based Algorithm in Fig. 4. It is observed that our proposed algorithm converges within four iterations. In the rest of the parts, the WPT performance is obtained by the SLA based algorithm. The impact of the phase-shifters' resolution on the output DC power is evaluated in Fig. 5, where the phase-shifters' resolution in both the IRS and that in the ER always keep the same. Observe from Fig. 5 that increasing the resolution of all the phase-shifters improves the output DC power. Furthermore, the output DC power of a single energy harvester with 3 bits resolution of phase-shifters and that of two energy harvesters with 4 bits resolution of phase-shifters achieve almost the same output DC power as the continuous counterparts, respectively. If we further increase the resolution of the phase-shifters, the output power only increases marginally.

Observe from Fig. 6 that, the output DC power increases as we increase the transmit power. Moreover, the output DC power with the aid of the IRS is always higher than a traditional MIMO system. For example, when the transmit power is 39 dBm, the output DC power associated with a single energy harvester is 3.60 dBm higher than the traditional MIMO counterpart. Furthermore, the output DC power increases slowly with a high transmit power. The output DC power of the IRS-aided WPT system with a single energy harvester increases slowly, when the transmit power is higher than 40 dBm. This is because the resultant RF power input to the energy harvester is in the saturation region. However, when two energy harvesters are implemented at the ER, the

This article has been accepted for publication in IEEE Transactions on Wireless Communications. This is the author's version which has not been fully edited and content may change prior to final publication. Citation information: DOI 10.1109/TWC.2023.3251743

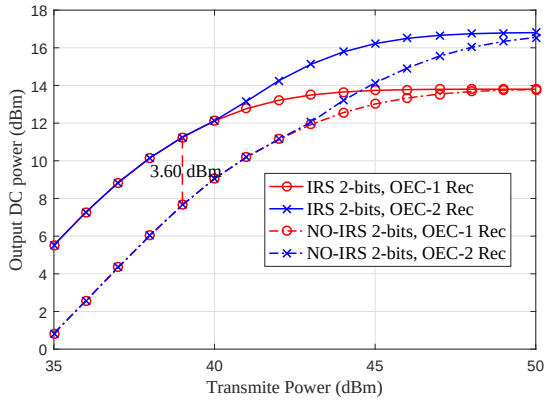

Fig. 6. Transmit power vs output power when $N_t = 4$,$N_r = 3$,$M = 100$.

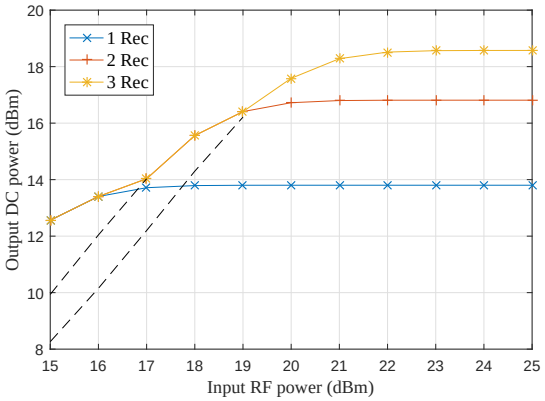

Fig. 8. Number of energy harvesters vs output power

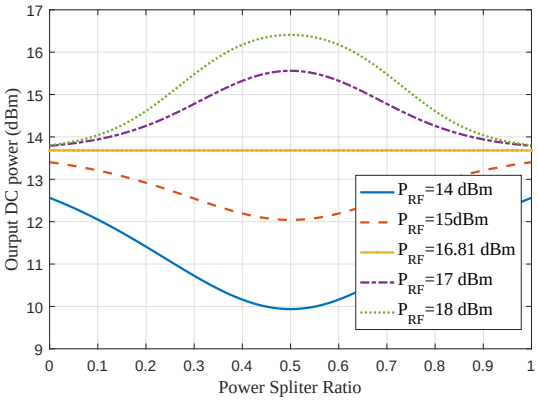

Fig. 7. Power spliter ratio vs output power

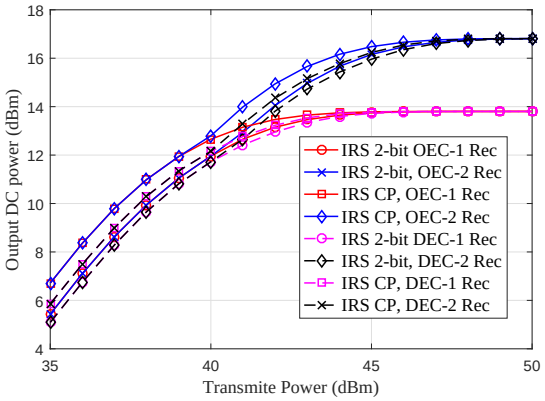

Fig. 9. Different schemes vs output power when $N_t = 4$,$N_r = 3$,$M = 100$.

output DC power in the IRS-aided WPT system with 2 energy harvesters still keeps a rapid growth. Since the received RF power is split into two portions, the RF power carried by every portion makes the energy harvester operate in the region with a high RF-DC efficiency. Furthermore, as shown in Fig. 6 the IRS-aided WPT system, with two energy harvesters doubles the saturated DC output power with a single energy harvester.

C. The Impact of Different ER

We investigate the impact of the power splitter on the output DC power in Fig. 7, where $N = 2$ energy harvesters are conceived. Observe from Fig. 7 that the output DC power keeps unchanged as we increase the power splitting ratio, when the input RF power is 16.81 dBm. This is because the RF-DC efficiency of a single and a pair energy harvesters are the same. When the input RF power is lower than 16.81 dBm, the power splitting ratio $\rho = 1$ or 0 achieves the highest output DC power. When the input RF power is 17 and 18 dBm, the output DC powers are both equal to 13.8 dBm, when $\rho = 0$ and 1. This is because the input RF power is sufficiently large to let the energy harvester operating the the saturation region. The highest output DC power is obtained by uniform power splitter with $\rho = 0.5$. We also observe from Fig. 7 that the power splitting ratio $\rho = 0.5$ is always the extreme point, which demonstrates our theoretical analysis in Section III-D.

Observing form Fig 8, the 3 Rec has best performance, since it is flexible to adjust the number of energy harvesters and power splitter. The dotted line is the ER uniform split the input RF power. We observe that the ER only use few energy harvesters when the input RF power is low. For example, the EU uses one energy harvester when the input RF power is 16 dBm.

Direct energy combiner (DEC) simply combines the RF signals received by the multiple antennas without any phase adjustment. The DEC can be denoted as $\mathbf{w}_{DEC} = [1, 1, \cdots, 1]$. Obviously, the OEC aims for achieving the optimal WPT performance, while the DEC sacrifices the WPT performance to some extent for a low implementation complexity. Observe from Fig. 9 that the continuous phase-shifters without any resolution constraints achieve higher WPT performance than low-resolution phase-shifters. For example, when our optimised energy combiner (OEC) is adopted and a single energy harvester is implemented at the ER, with a transmit power of 40 dBm, the continuous phase-shifters of the IRS and the ER achieve an output DC power 1 dBm higher than the 2-bit phase-shifters.

Observe from Fig. 9 that our OEC outperforms the DEC. Specifically, the output DC power of the OEC scheme with a single energy harvester and continuous IRS is 1.51 dBm higher than that of the DEC scheme. This is because the DEC scheme can not fully exploit the spatial gain. Furthermore, the DEC architecture with 2 energy harvester are illustrated in Fig. 9. We observe from this figure that DEC with 2 energy harvester harvest more energy than that with 1 energy harvester. This is because DEC with 2 energy harvester can

split the high input RF power in order to keep these two energy harvesters working with high RF-DC conversation efficiencies. By contrast, DEC with a single energy harvester may operate in the saturation region, when the input RF power is very high. Moreover, DEC with 2 energy harvester harvest less energy than OEC with 2 energy harvester due to the destructive energy combining, when the RF signals gleaned by the received antennas have different phases. Moreover, when the transmit power is lower than 40 dBm, the OEC with a single energy harvester has same performance with its counterpart with two energy harvesters. When the transmit power is higher than 40 dBm, the OEC with two energy harvesters performs better.

VII. Conclusion

In this paper, we study an IRS-aided WPT system by conceiving a practical ER. The active transmit beamformer of the transmitter, the passive reflecting beamformer of the IRS, the energy combiner and the power splitter of the ER are jointly designed by considering low-resolution phase-shifters and multiple energy harvesters. Two algorithms, namely SLA and I-GRASP, are proposed to maximise the input RF power. Furthermore, the optimal power splitter for maximising the output DC power is derived in close-form. When the transmit power is 39 dBm, an IRS-aided output DC power is 3.60 mW higher than the traditional MIMO counterpart. The output DC power of two energy harvesters with 4 bits resolution phase-shifters achieves almost the same output DC power as the continuous counterparts.

The M-QAM waveforms are able to carry both energy and information simultaneously. Gaussian waveforms are regarded as an ideal model, which could be approached by the high order M-QAM waveforms. In the future work, we can investigate the impacts of M-QAM waveforms on simultaneously wireless information and power transfer.

Appendix A

We first consider the inequality of $F(\text{vec}(\mathbf{\Phi}_c{}^n)|\text{vec}(\mathbf{\Phi}_c{}^{n-1})) \geq F(\text{vec}(\mathbf{\Phi}_c{}^{n-1})|\text{vec}(\mathbf{\Phi}_c{}^{n-1}))$. The function $F(\text{vec}(\mathbf{\Phi}_c)^n|\text{vec}(\mathbf{\Phi}_c{}^{n-1}))$ can be expressed as

$$F(\text{vec}(\mathbf{\Phi}_c)^n|\text{vec}(\mathbf{\Phi}_c{}^{n-1})) = \text{Re}\{\text{vec}(\mathbf{\Phi}_c{}^{n-1})\mathbf{\Theta}\mathbf{\Theta}^H\text{vec}(\mathbf{\Phi}_c^n)^H + 2\mathbf{w}_c^H\mathbf{H}_d\mathbf{\Theta}^H\text{vec}(\mathbf{\Phi}_c^n)^H\}. \quad (48)$$

We then obtain $\mathbf{\Phi}_c^n$ by solving the following optimisation problem:

$$\text{(P4.1.2): } \max_{\mathbf{\Phi}_c^n} F(\text{vec}(\mathbf{\Phi}_c^n)|\text{vec}(\mathbf{\Phi}_c{}^{n-1})), \quad (49)$$

$$\text{s.t. } ||\text{vec}(\mathbf{\Phi}_c^n)(m)||^2 = 1 \; m = 1, \cdots, M. \quad (49a)$$

Note that $\mathbf{\Phi}_c^{n-1}$ is a feasible solution to (P4.1.2), while $\mathbf{\Phi}_c^n$ is the optimal one. Therefore, we obtain the inequality of $F(\text{vec}(\mathbf{\Phi}_c{}^n)|\text{vec}(\mathbf{\Phi}_c{}^{n-1})) \geq F(\text{vec}(\mathbf{\Phi}_c{}^{n-1})|\text{vec}(\mathbf{\Phi}_c{}^{n-1}))$.

Next we consider the inequality $F(\text{vec}(\mathbf{\Phi}_c{}^n)|\text{vec}(\mathbf{\Phi}_c{}^n)) \geq F(\text{vec}(\mathbf{\Phi}_c{}^n)|\text{vec}(\mathbf{\Phi}_c{}^{n-1}))$. Note that $F(\text{vec}(\mathbf{\Phi}_c{}^n)|\text{vec}(\mathbf{\Phi}_c{}^n)) - F(\text{vec}(\mathbf{\Phi}_c{}^n)|\text{vec}(\mathbf{\Phi}_c{}^{n-1})) = \text{Re}\{\text{vec}(\mathbf{\Phi}_c{}^n)\mathbf{\Theta}\mathbf{\Theta}^H\text{vec}(\mathbf{\Phi}_c^n)^H\} - \text{Re}\{\text{vec}(\mathbf{\Phi}_c{}^{n-1})\mathbf{\Theta}\mathbf{\Theta}^H\text{vec}(\mathbf{\Phi}_c^n)^H\}$. Observe from this equation that $\mathbf{\Theta}^H\text{vec}(\mathbf{\Phi}_c^n)^H$ is a complex number, while both $\mathbf{\Phi}_c^{n-1}$ and $\mathbf{\Phi}_c^n$ have the same norms. Therefore, the value of the conjugate transpose of $\mathbf{\Phi}_c^n$ is larger than that of $\mathbf{\Phi}_c^{n-1}$. As a result, we have $F(\text{vec}(\mathbf{\Phi}_c{}^n)|\text{vec}(\mathbf{\Phi}_c{}^n)) \geq F(\text{vec}(\mathbf{\Phi}_c{}^n)|\text{vec}(\mathbf{\Phi}_c{}^{n-1}))$.

Appendix B
Proof of proposition 1

The proof can be finished in the following steps:

Step 1: We prove the optimal objective value of (P4.1.3) is the upper bound to (P4.1.2). According to (P4.1.2), when $\mathbf{\Phi}_c$ is a feasible solution, it satisfies $||\text{vec}(\mathbf{\Phi}_c)(m)||_2^2 = 1$, $\forall m = 1, \cdots, M$. This is also a feasible solution to (P4.1.3), since it also satisfis $||\text{vec}(\mathbf{\Phi}_c)(m)||_2^2 \leq 1, \forall m = 1, \cdots, M$. Since all the feasible solutions to (P4.1.2) are also feasible to (P4.1.3), the optimal objective value of (P4.1.3) is the upper bound to (P4.1.2).

Step 2: We prove that the optimal solution of (P4.1.3) satisfies the unit-modulus constraint of (P4.1.2). Let us suppose that $\mathbf{\Phi}_c'$ is a feasible solution to (P4.1.3), but some of its elements do not satisfy the unit-modulus constraint of (P4.1.2). Let us define a set $\mathcal{S} = \{\mathbf{\Phi}_c'(j), \forall j = 1, 2, \cdots, M| \; ||\mathbf{\Phi}_c'(j)||^2 < 1\}$. This set contains the elements in a feasible solution $\mathbf{\Phi}_c'$ which violate the unit-modulus constraint. We can always find a better solution $\hat{\mathbf{\Phi}}_c$, which is expressed as

$$\hat{\mathbf{\Phi}}_c = \begin{cases} \mathbf{\Phi}_c'(j), \text{for } \forall \; j \notin \mathcal{S}, \\ k_j\mathbf{\Phi}_c'(j), \; j \in \mathcal{S}. \end{cases} \quad (50)$$

If $(\mathbf{a}(j) + \mathbf{b}(j))\mathbf{\Phi}_c'(j) > 0$, we set $k_j = 1/\mathbf{\Phi}_c'(j)$. Otherwise, we set $k_j = -1/\mathbf{\Phi}_c'(i)$,where we have $\mathbf{a} = \text{vec}(\mathbf{\Phi}_c{}^{n-1})\mathbf{\Theta}\mathbf{\Theta}^H$ and $\mathbf{b} = \mathbf{w}^*\mathbf{H}_d^H\mathbf{\Theta}$. The performance difference between $\hat{\mathbf{\Phi}}_c'$ and that of $\mathbf{\Phi}_c'$ is derived as

$$F(\hat{\mathbf{\Phi}}_c|\mathbf{\Phi}_c^{n-1}) - F(\mathbf{\Phi}_c'|\mathbf{\Phi}_c^{n-1}) = \sum_{j\in\mathcal{S}}(k_j - 1)(\mathbf{a}(j) + \mathbf{b}(j))\mathbf{\Phi}_c'(j) > 0. \quad (51)$$

Therefore, for any feasible solution $\mathbf{\Phi}_c'$ to (P4.1.3), it cannot be optimal, when it does not satisfy the unit-modulus constraint. This is because we may always find a better solution $\hat{\mathbf{\Phi}}_c$, according to Eq. (51). In a nutshell, we prove that the optimal solution to (P4.1.3) should also satisfy the unit-modulus constraint of (P4.1.2).

Step 3: Both (P4.1.3) and (P4.1.2) only have a single optimal solution. There is only a single optimal solution $\mathbf{\Phi}_c^*$ to (P4.1.3), due to its convexity. According to Step 2, $\mathbf{\Phi}_c^*$ is also an optimal solution to (P4.1.2). Let us assume that (P4.1.2) also has another multiple optimal solutions $\{\mathbf{\Phi}_c^1, \cdots, \mathbf{\Phi}_c^k\}$. Note that these solutions are different from $\mathbf{\Phi}_c^*$, while they all satisfy the unit-modulus constraint. Therefore, $\{\mathbf{\Phi}_c^1, \cdots, \mathbf{\Phi}_c^k\}$ and $\mathbf{\Phi}_c^*$ should achieve exactly the same value of the objective function in (P4.1.2). Obviously, $\{\mathbf{\Phi}_c^1, \cdots, \mathbf{\Phi}_c^k\}$ satisfy the constraint of $||\text{vec}(\mathbf{\Phi}_c{}^i)(m)||_2^2 \leq 1, \forall i = 1, 2, \cdots, k$, they are all feasible to $(P4.1.3)$. Therefore, $\{\mathbf{\Phi}_c^1, \cdots, \mathbf{\Phi}_c^k\}$ and $\mathbf{\Phi}_c^*$ are all optimal solutions to (P4.1.3). Eventually, this conclusion results in a conflict to the fact that (P4.1.3) only has a single optimal solution. Therefore, our assumption does not hold, while (P4.1.2) also has a single optimal solution.

From Steps 1 and 2, the optimal solution of (P4.1.3) is also optimal to (P4.1.2). These two optimisation problems have the same solution due to its uniqueness, according to Step 3.

APPENDIX C
CONVERGENCE OF ALGORITHM 3

Since the the objective function is continuous and the constraints are continuous and in the closed interval, the optimum has a upper bound. During the $(n-1)$-th iteration, the input of Algorithm 1 is $\{\mathbf{f}^{n-1}, {\mathbf{w}_c}^{n-1}\}$ and ${\mathbf{\Phi}_c}^{n-1}$, which yields the objective value $F(\mathbf{f}^{n-1}, {\mathbf{w}_c}^{n-1}, {\mathbf{\Phi}_c}^{n-1})$. The output of Algorithm 1, which is also the input of Algorithm 2 is $\{\mathbf{f}^{n-1}, {\mathbf{w}_c}^{n-1}, {\mathbf{\Phi}_c}^{n}\}$. Since the objective value of (P3.1) is monotonously increases after every iteration in Algorithm 1, we have $F(\mathbf{f}^{n-1}, {\mathbf{w}_c}^{n-1}, {\mathbf{\Phi}_c}^{n}) > F(\mathbf{f}^{n-1}, {\mathbf{w}_c}^{n-1}, {\mathbf{\Phi}_c}^{n-1})$. The output of Algorithm 2 are $\{\mathbf{f}^{n}, {\mathbf{w}_c}^{n}, {\mathbf{\Phi}_c}^{n}\}$. Similarly, we also have $F(\mathbf{f}^{n}, {\mathbf{w}_c}^{n}, {\mathbf{\Phi}_c}^{n}) > F(\mathbf{f}^{n-1}, {\mathbf{w}_c}^{n-1}, {\mathbf{\Phi}_c}^{n-1})$. Therefore, the objective value of P(3) monotonously increases. The convergence of Algorithm 3 is proved. Define $\{\mathbf{f}^*, {\mathbf{w}_c}^*, {\mathbf{\Phi}_c}^*\}$ as the ultimate outputs of Algorithm 3. According to Algorithm 1, it satisfies the following conditions expressed as

$$\begin{cases} \boldsymbol{\lambda}(i) \geq 0 \ i = 1, 2, \cdots, M \\ \boldsymbol{\lambda}(i)(\text{vec}({\mathbf{\Phi}_c}^*)(i)(\text{vec}({\mathbf{\Phi}_c}^*)(i))^H - 1) = 0 \ i = 1, 2, \cdots, M \\ \mathbf{a}(i) + \mathbf{b}(i) + \boldsymbol{\lambda}(i)\text{vec}(\mathbf{\Phi}_c)^*(i) = 0 \ i = 1, 2, \cdots, M \end{cases} \tag{52}$$

where $\mathbf{a} = (\text{vec}(\mathbf{\Phi}_c)^*)\mathbf{\Theta}\mathbf{\Theta}^H$, $\mathbf{b} = \mathbf{w}^*\mathbf{H}_d^H\mathbf{\Theta}^H$ and $\mathbf{\Theta} = diag({\mathbf{w}_c^*}^H\mathbf{G})\mathbf{H}_r\mathbf{f}^*$.

According to Algorithm 2, the output of Algorithm 3 satisfies the following conditions expressed as

$$\begin{cases} \boldsymbol{\mu}(i) \geq 0, \ i = 1, 2, \cdots, M, \\ \boldsymbol{\mu}(i)({\mathbf{w}_c}^*(i)({\mathbf{w}_c}^*(i))^H - 1) = 0, \ i = 1, 2, \cdots, N_r, \\ \boldsymbol{\beta}(i)^H + \boldsymbol{\mu}(i){\mathbf{w}_c}^*(i) = 0, \ i = 1, 2, \cdots, N_r. \end{cases} \tag{53}$$

where $\boldsymbol{\beta} = ({\mathbf{w}_c}^*)^H(\mathbf{H}_d + \mathbf{G}\mathbf{\Phi}_c^*\mathbf{H}_r)(\mathbf{H}_d + \mathbf{G}\mathbf{\Phi}_c^*\mathbf{H}_r)^H$. By jointly considering Eq. (52) and Eq. (53), we find that the optimal solution $\{\mathbf{f}^*, {\mathbf{w}_c}^*, {\mathbf{\Phi}_c}^*\}$ satisfies the KKT condition of (P3).

APPENDIX D
PROOF OF PROPOSITION 2

The extreme value of $f_N(\boldsymbol{\rho})$ is $N\Psi(1/N * P_{RF})$. When $N \to \infty$, the derivative of $(N\Psi(1/N * P_{RF})$ with respect to N tends to zero, which can be demonstrated by the following derivation:

$$\begin{aligned} &\lim_{N\to\infty} \frac{\mathrm{d}(N\Psi(1/N * P_{RF}))}{\mathrm{d}N} \\ =&\lim_{N\to\infty} \frac{M}{X(1+\exp(-a(1/N * P_{RF} - b)))} - Y \\ &+ \frac{-MaP_{RF}\exp(-a(1/N * P_{RF} - b))}{NX[1+\exp(-a(1/N * P_{RF} - b))]^2} \\ =&0 \end{aligned}$$

where $X = \frac{\exp(ab)}{1+\exp(ab)}$ and $Y = \frac{M}{\exp(ab)}$.

REFERENCES

[1] J. Hu, Q. Wang, and K. Yang, "Energy Self-Sustainability in Full-Spectrum 6G," *IEEE Wireless Communications*, vol. 28, no. 1, pp. 104–111, 2021.

[2] H. J. Visser and R. J. M. Vullers, "RF Energy Harvesting and Transport for Wireless Sensor Network Applications: Principles and Requirements," *Proceedings of the IEEE*, vol. 101, no. 6, pp. 1410–1423, 2013.

[3] J. Hu, K. Yang, G. Wen, and L. Hanzo, "Integrated Data and Energy Communication Network: A Comprehensive Survey," *IEEE Communications Surveys Tutorials*, vol. 20, no. 4, pp. 3169–3219, 2018.

[4] S. Zhong and X. Wang, "Wireless Power Transfer by Beamspace Large-Scale MIMO With Lens Antenna Array," *IEEE Transactions on Wireless Communications*, vol. 18, no. 2, pp. 1390–1403, 2019.

[5] E. Boshkovska, D. W. K. Ng, N. Zlatanov, and R. Schober, "Practical Non-Linear Energy Harvesting Model and Resource Allocation for SWIPT Systems," *IEEE Communications Letters*, vol. 19, no. 12, pp. 2082–2085, 2015.

[6] K. Xiong, B. Wang, and K. J. R. Liu, "Rate-Energy Region of SWIPT for MIMO Broadcasting Under Nonlinear Energy Harvesting Model," *IEEE Transactions on Wireless Communications*, vol. 16, no. 8, pp. 5147–5161, 2017.

[7] Y. Lu, K. Xiong, P. Fan, Z. Ding, Z. Zhong, and K. B. Letaief, "Global Energy Efficiency in Secure MISO SWIPT Systems With Non-Linear Power-Splitting EH Model," *IEEE Journal on Selected Areas in Communications*, vol. 37, no. 1, pp. 216–232, 2019.

[8] J. Park and B. Clerckx, "Joint Wireless Information and Energy Transfer With Reduced Feedback in MIMO Interference Channels," *IEEE Journal on Selected Areas in Communications*, vol. 33, no. 8, pp. 1563–1577, 2015.

[9] C. Song and Y. Jeon, "Weighted MMSE Precoder Designs for Sum-Utility Maximization in Multi-User SWIPT Network-MIMO With Per-BS Power Constraints," *IEEE Transactions on Vehicular Technology*, vol. 67, no. 3, pp. 2809–2813, 2018.

[10] D. Mishra and G. C. Alexandropoulos, "Transmit Precoding and Receive Power Splitting for Harvested Power Maximization in MIMO SWIPT Systems," *IEEE Transactions on Green Communications and Networking*, vol. 2, no. 3, pp. 774–786, 2018.

[11] J. P. M. G. Linnartz, Y. Wu, J. G. A. Mare, and M. K. Matters-Kammerer, "Multiple Antenna Rectifiers for Radio Frequency Energy Scavenging in Wireless Sensors," in *2015 IEEE International Symposium on Circuits and Systems (ISCAS)*, pp. 702–705, 2015.

[12] S. Shen and B. Clerckx, "Beamforming Optimization for MIMO Wireless Power Transfer With Nonlinear Energy Harvesting: RF Combining Versus DC Combining," *IEEE Transactions on Wireless Communications*, vol. 20, no. 1, pp. 199–213, 2021.

[13] Q. Wu and R. Zhang, "Towards Smart and Reconfigurable Environment: Intelligent Reflecting Surface Aided Wireless Network," *IEEE Communications Magazine*, vol. 58, no. 1, pp. 106–112, 2020.

[14] C. Pan, H. Ren, K. Wang, J. F. Kolb, M. Elkashlan, M. Chen, M. Di Renzo, Y. Hao, J. Wang, A. L. Swindlehurst, X. You, and L. Hanzo, "Reconfigurable Intelligent Surfaces for 6G Systems: Principles, Applications, and Research Directions," *IEEE Communications Magazine*, vol. 59, no. 6, pp. 14–20, 2021.

[15] T. J. Cui, M. Q. Qi, X. Wan, J. Zhao, and Q. Cheng, "Coding metamaterials, digital metamaterials and programmable metamaterials," *Light Science & Applications*, vol. 3, no. 10, p. e218, 2014.

[16] T. Bai, C. Pan, H. Ren, Y. Deng, M. Elkashlan, and A. Nallanathan, "Resource Allocation for Intelligent Reflecting Surface Aided Wireless Powered Mobile Edge Computing in OFDM Systems," *IEEE Transactions on Wireless Communications*, vol. 20, no. 8, pp. 5389–5407, 2021.

[17] C. Pan, H. Ren, K. Wang, M. Elkashlan, A. Nallanathan, J. Wang, and L. Hanzo, "Intelligent Reflecting Surface Aided MIMO Broadcasting for Simultaneous Wireless Information and Power Transfer," *IEEE Journal on Selected Areas in Communications*, pp. 1–1, 2020.

[18] B. Lyu, D. T. Hoang, S. Gong, and Z. Yang, "Intelligent Reflecting Surface Assisted Wireless Powered Communication Networks," in *2020 IEEE Wireless Communications and Networking Conference Workshops (WCNCW)*, pp. 1–6, 2020.

[19] Q. Wu and R. Zhang, "Weighted Sum Power Maximization for Intelligent Reflecting Surface Aided SWIPT," *IEEE Wireless Communications Letters*, vol. 9, no. 5, pp. 586–590, 2020.

[20] Q. Wu and R. Zhang, "Beamforming Optimization for Wireless Network Aided by Intelligent Reflecting Surface With Discrete Phase Shifts," *IEEE Transactions on Communications*, vol. 68, no. 3, pp. 1838–1851, 2020.

[21] S. Gong, Z. Yang, C. Xing, J. An, and L. Hanzo, "Beamforming Optimization for Intelligent Reflecting Surface-Aided SWIPT IoT Networks Relying on Discrete Phase Shifts," *IEEE Internet of Things Journal*, vol. 8, no. 10, pp. 8585–8602, 2021.

[22] Z. Abdullah, G. Chen, S. Lambotharan, and J. Chambers, "Low-Complexity Antenna Selection and Discrete Phase-Shifts Design in IRS-Assisted Multiuser Massive MIMO Networks," *IEEE Transactions on Vehicular Technology*, pp. 1–1, 2022.

[23] X. Hu, L. Jin, K. Huang, X. Sun, Y. Zhou, and J. Qu, "Intelligent Reflecting Surface-Assisted Secret Key Generation With Discrete Phase Shifts in Static Environment," *IEEE Wireless Communications Letters*, vol. 10, no. 9, pp. 1867–1870, 2021.

[24] Q. Wu and R. Zhang, "Intelligent reflecting surface enhanced wireless network via joint active and passive beamforming," *IEEE Transactions on Wireless Communications*, vol. 18, no. 11, pp. 5394–5409, 2019.

[25] C. Pan, H. Ren, K. Wang, W. Xu, M. Elkashlan, A. Nallanathan, and L. Hanzo, "Multicell MIMO Communications Relying on Intelligent Reflecting Surfaces," *IEEE Transactions on Wireless Communications*, vol. 19, no. 8, pp. 5218–5233, 2020.

[26] D. R. Hunter and K. Lange, "A Tutorial on MM Algorithms," *American statian*, vol. 58, no. 1, pp. pags. 30–37, 2004.

[27] Y. Sun, P. Babu, and D. P. Palomar, "Majorization-Minimization Algorithms in Signal Processing, Communications, and Machine Learning," *IEEE Transactions on Signal Processing*, vol. 65, no. 3, pp. 794–816, 2017.

[28] R. Burkard, M. Dell'Amico, and S. Martello, *Assignment Problems*. Society for Industrial and Applied Mathematics, 2012.

[29] E. Cela, "The Quadratic Assignment Problem," *INFORMS*, 1963.

[30] T. My, P. Mpy, L. S. Pitsoulis, and M. Resende, "A GRASP for the biquadratic assignment problem," *European Journal of Operational Research*, vol. 105, no. 3, pp. 613–621, 1998.

[31] Y. Lu, K. Xiong, P. Fan, Z. Ding, Z. Zhong, and K. B. Letaief, "Global Energy Efficiency in Secure MISO SWIPT Systems With Non-Linear Power-Splitting EH Model," *IEEE Journal on Selected Areas in Communications*, 2019.

[32] U. Olgun, C.-C. Chen, and J. L. Volakis, "Investigation of Rectenna Array Configurations for Enhanced RF Power Harvesting," *IEEE Antennas and Wireless Propagation Letters*, vol. 10, pp. 262–265, 2011.

[33] G. T. de Araujo, A. L. F. de Almeida, and R. Boyer, "Channel Estimation for Intelligent Reflecting Surface Assisted MIMO Systems: A Tensor Modeling Approach," *IEEE Journal of Selected Topics in Signal Processing*, vol. 15, no. 3, pp. 789–802, 2021.

[34] O. T. Demir and E. Björnson, "Joint power control and LSFD for wireless-powered cell-free massive MIMO," *IEEE Transactions on Wireless Communications*, vol. 20, no. 3, pp. 1756–1769, 2021.

Qingdong Yue received his B.S degree from Chongqing Univesity (CQU), China, in 2018. He is now studying for a Ph.D. degree at University of Electronic Science and Technology of China (UESTC). His research interests include simultaneous wireless information and power transfer, MIMO and intelligent reflecting surface.

Jie Hu [S'11, M'16, SM'21] (hujie@uestc.edu.cn) received his B.Eng. and M.Sc. degrees from Beijing University of Posts and Telecommunications, China, in 2008 and 2011, respectively, and received the Ph.D. degree from the School of Electronics and Computer Science, University of Southampton, U.K., in 2015. Since March 2016, he has been working with the School of Information and Communication Engineering, University of Electronic Science and Technology of China (UESTC). He is now a Research Professor and PhD supervisor. He won UESTC's Academic Young Talent Award in 2019. Now he is supported by the "100 Talents" program of UESTC. He is an editor for *IEEE Wireless Communications Letters*, *IEEE/CIC China Communications* and *IET Smart Cities*. He serves for *IEEE Communications Magazine*, *Frontiers in Communications and Networks* as well as *ZTE communications* as a guest editor. He is a technical committee member of ZTE Technology. He is a program vice-chair for IEEE TrustCom 2020, a technical program committee (TPC) chair for IEEE UCET 2021 and a program vice-chair for UbiSec 2022. He also serves as a TPC member for several prestigious IEEE conferences, such as IEEE Globecom/ICC/WCSP and etc. He has won the best paper award of IEEE SustainCom 2020 and the best paper award of IEEE MMTC 2021. His current research focuses on wireless communications and resource management for B5G/6G, wireless information and power transfer as well as integrated communication, computing and sensing.

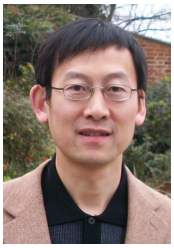

Kun Yang [M'00, SM'10, F'23] received his PhD from the Department of Electronic & Electrical Engineering of University College London (UCL), UK. He is a Chair Professor in the School of Computer Science & Electronic Engineering, University of Essex, leading the Network Convergence Laboratory (NCL), UK. He is also an affiliated professor at UESTC, China. Before joining in the University of Essex at 2003, he worked at UCL on several European Union (EU) research projects for several years. His main research interests include wireless networks and communications, IoT networking, data and energy integrated networks and mobile computing. He manages research projects funded by various sources such as UK EPSRC, EU FP7/H2020 and industries. He has published 200+ journal papers and filed 20 patents. He serves on the editorial boards of both IEEE (e.g., IEEE TNSE, WCL, ComMag) and non-IEEE journals. He is an IEEE ComSoC Distinguished Lecturer (2020-2021) and a Member of Academia Europaea (MAE).

Qin Yu received the B.S. degree in communication engineering from the Chongqing University of Posts and Telecommunications, Chongqing, China, in 1996, and the M.S. and Ph.D. degrees in communication and information engineering from the University of Electronic Science and Technology of China (UESTC), Chengdu, China, in 2002 and 2006, respectively. She joined the School of Communication and Information Engineering, UESTC, in 2007, where she conducted post-doctoral research in information security from 2007 to 2009. Her current interests include wireless communication and mobile networking, such as data and energy integrated communication networks, wireless resources allocation, communication and computation convergence.